Tero Tynjälä

THEORETICAL AND NUMERICAL STUDY OF THERMOMAGNETIC CONVECTION IN MAGNETIC FLUIDS

Thesis for the degree of Doctor of Science (Technology) to be presented with due permission for public examination and criticism in the Auditorium 1382 at Lappeenranta University of Technology, Lappeenranta, Finland, on the 14th of October, 2005, at noon.

Acta Universitatis
Lappeenrantaensis
220

Supervisor Professor Pertti Sarkomaa
Department of Energy and Environmental Technology
Lappeenranta University of Technology
Finland

Reviewers Professor Elmars Blums
Institute of Physics
University of Latvia
Latvia

Professor Yuriy L. Raikher
Institute of Continuous Media Mechanics
Ural Branch of the Russian Academy of Sciences
Russia

Opponent Professor Elmars Blums
Institute of Physics
University of Latvia
Latvia

ISBN 952-214-109-7
ISSN 1456-4491
Lappeenrannan teknillinen yliopisto
Digipaino 2005

Abstract

Tero Tynjälä

Theoretical and numerical study of thermomagnetic convection in magnetic fluids

Lappeenranta 2005

95 pages

Acta Universitatis Lappeenrantaensis 220

Diss. Lappeenranta University of Technology

ISBN 952-214-109-7, ISSN 1456-4491

Magnetic fluids consist of magnetic particles suspended in an appropriate carrier liquid. The novelty of the magnetic fluids is that the fluid flow and apparent fluid properties may be controlled by an external magnetic field. Since the discovery of the unique properties of magnetic fluids, several applications for magnetic fluids have been considered. The variety of applications is diverse, ranging from technical and biomedical to scientific applications. The physics of magnetic fluids is a highly multi-disciplinary topic, which combines statistical mechanics and magnetism with hydrodynamics. The size of the magnetic particles in stable magnetic fluids varies from a few to tens of nanometers. The particle size range is only about an order of magnitude larger than the molecular scale. Therefore, magnetic fluids are a potential candidate for currently intensively studied microfluidic and nanotechnology applications.

In this thesis, the magnetic field control of convection instabilities and heat and mass transfer processes in magnetic fluids have been investigated by numerical simulations and theoretical considerations. Simulation models based on finite element and finite volume methods have been developed. In addition to standard conservation equations, the magnetic field inside the simulation domain is calculated from Maxwell equations and the necessary terms to take into account for the magnetic body force and magnetic dissipation have been added to the equations governing the fluid motion. In order to study the effect of non-homogeneous particle distribution on magnetic fluid convection, the simulations have been carried out by using both single phase and two-phase mixture models. The simulation models have been tested against available experimental results and qualitatively good results have been achieved. Detailed quantitative comparison of simulation results with the experiments is often problematic because of the lack of information about the fluid properties. Even if the fluids are synthesized and analyzed in the laboratory where the experiments are performed, the magnetic fluid particles are not monodisperse and the fluid properties are averaged mean

values.

Based on numerical simulations, the size of the drop aggregates, which could lead to experimentally observed sedimentation, was found to be the order of 100 nm or larger, which is clearly more than the commonly accepted value for magnetic fluids of good quality. Numerical simulations of magnetic fluid convection near the threshold supported experimental observations qualitatively. Near the onset of convection the competitive action of thermal and concentration density gradients leads to mostly spatiotemporally chaotic convection with oscillatory and travelling wave regimes, previously observed in binary mixtures and nematic liquid crystals. Oscillatory convection was observed in the entire investigated temperature region and different wave regimes, such as spirals, targets, rolls and cross-rolls, were discovered. The existence of large and small periods is typical for magnetic fluid convection. Experimentally observed hysteresis and strong dependence of the measured heat flux on the prehistory of the experiments alludes to a non-newtonian nature of magnetic fluids.

In many applications of magnetic fluids, the heat and mass transfer processes including the effects of external magnetic fields are of great importance. In addition to magnetic fluids, the concepts and the simulation models used in this study may be applied also to the studies of convective instabilities in ordinary fluids as well as in other binary mixtures and complex fluids.

Keywords: magnetic fluid, magnetic convection, mixture model
UDC 536.255 : 621.318.1 : 532.517 : 544.034

Preface

This study has been carried out between 1999 and 2005 in the Laboratory of the Thermodynamics of the Department of Energy and Environmental Technology at the Lappeenranta University of Technology.

I would like to express my gratitude to my supervisor, Professor Pertti Sarkomaa, Head of the Laboratory of Thermodynamics, for his encouragement during the research.

I wish to thank Professor Gennady Putin and Dr. Alexandra Bozhko from the Department of Physics of Perm State University for fruitful cooperation. Especially the experimental results they provided were essential for the progress of my studies.

The pre-examiners Professor Elmars Blums and Professor Yuriy L. Raikher deserve special thanks for their careful reviews and insightful comments.

I am also deeply indebted to Professor Piroz Zamankhan for his guidance and friendship throughout my studies. I also wish to thank all my former and present colleagues and friends in the Department of Energy and Environmental Technology. I would especially like to mention Dr. Payman Jalali, Mr. Visa Poikolainen and Mr. Jouni Ritvanen, who helped me in numerous stages of this study. I am truly sorry that Visa is not here with his carefully thought comments. I am sure that he would have had lot to say about the formulation of the conservation equations, the field he mastered better than most of us.

This work has been funded by the Academy of Finland, the Foundation of the Lappeenranta University of Technology, the Foundation of Technology in Finland and the South-Carelian Fund of the Finnish Cultural Foundation. The financial supports and the computing time provided by the CSC - Scientific Computing Ltd., the Finnish IT center for science, are gratefully acknowledged.

Finally, and most of all, I am grateful to Katja and Tuuli, who remind me every day that there is so much more to life than physics.

Lappeenranta, September 2005.

Tero Tynjälä

Don't model bulldozers with quarks
(Goldenfeld and Kadanoff, 1999)

Contents

List of Publications

Publication I

T. Tynjälä, A. Bozhko, P. Bulychev, G. Putin, and P. Sarkomaa. On features of ferrofluid convection caused by barometrical sedimentation. *Journal of Magnetism and Magnetic Materials*, 2005. (Accepted for publication)

This paper is cowork with Dr. Bozhko, Prof. Putin and Mr. Bulychev from Perm State University. Group of Prof. Putin from Perm State University is responsible for the experiments and Mr. Tynjälä conducted the computer simulations. Discussion and conclusions were written together with all contributing authors.

Publication II

A. Bozhko, T. Tynjälä. Influence of sedimentation of magnetic particles on ferrofluid convection in experiments and numerical simulations. *Journal of Magnetism and Magnetic Materials* Vol. 289, pp. 281–284, 2005.

Mr. Tynjälä is corresponding author of this paper. The paper is cowork with Dr. Bozhko from Perm State University. Dr. Bozhko is responsible for the experiments and Mr. Tynjälä conducted the computer simulations. Theory, discussion and conclusions were written together with Dr. Bozhko.

Publication III

A. Bozhko, G. Putin and T. Tynjälä. Oscillatory regimes of Rayleigh convection in ferrofluid. *Notices of Universities, South of Russia, Natural Sciences, Special Issue*, pp. 68–73, 2004.

This paper is cowork with Dr. Bozhko and Prof. Putin from Perm State University. Dr. Bozhko is responsible for the experiments and Mr. Tynjälä conducted the computer simulations. Theory, discussion and conclusions were written and reviewed together by Dr. Bozhko, Prof. Putin and Mr. Tynjälä.

Publication IV

A. Bozhko, G. Putin, P. Bulychev, T. Tynjälä and P. Sarkomaa. Experimental and numerical study of oscillatory convection in ferrofluids. *Joint 15th Riga and 6th PAMIR International Conference on Fundamental and Applied MHD*, Riga Jurmala, Latvia, June 27 - July 1. Vol. 1, pp. 337–340, 2005.

This presentation is cowork with Dr. Bozhko, Prof. Putin and Mr. Bulychev from Perm State University. Dr. Bozhko is responsible for the experiments and Mr. Tynjälä conducted the computer simulations. Discussion

and conclusions were written together with all contributing authors.

Publication V

T. Tynjälä, J. Ritvanen. Simulations of thermomagnetic convection in an annulus between two concentric cylinders. *Indian Journal of Engineering & Material Sciences*, Vol. 11, pp. 283–288, 2004.

Mr. Tynjälä is corresponding author of this paper. Mr. Ritvanen reviewed the paper and helped with postprocessing the simulation results and preparing the figures for the publication.

Publication VI

T. Tynjälä, A. Hajiloo, W. Polashenski Jr. and P. Zamankhan. Magnetodissipation in ferrofluids. *Journal of Magnetism and Magnetic Materials*, Vol. 252, pp. 123–125, 2002.

Mr. Tynjälä is corresponding author of this paper. Prof. Zamankhan advised with the derivation of the required equations and Dr. Hajiloo helped implementing the simulation code in practise.

Publication VII

P. Jalali, W. Polashenski Jr., T. Tynjälä and P. Zamankhan. Particle interactions in a dense monosized granular flow. *Physica D*, Vol. 162, pp. 188–207, 2002.

Corresponding author of the paper is Dr. Jalali. Theory and simulation code were developed mainly by Dr. Jalali and Prof. Zamankhan. Contribution of Mr. Tynjälä is limited to running the simulations, gathering the simulation data and postprocessing the results.

Publication VIII

Piroz Zamankhan, T. Tynjälä, W. Polashenski Jr., Parsa Zamankhan and P. Sarkomaa. Stress fluctuations in continuously sheared dense granular materials. *Physical Review E*, Vol. 60, pp. 7149–7156, 1999.

Corresponding author of the paper is Prof. Zamankhan, who also developed the code used in the simulations. Contribution of Mr. Tynjälä is limited to running the simulations, gathering the simulation data and postprocessing the results.

Nomenclature

Capital letters

B	magnetic flux density	$\mathrm{T}, \mathrm{Wb/m^2}$
C	heat capacity	J/K
$C(a,b)$	wavelet transform of a function	–
C_D	drag coefficient	–
D	diffusion coefficient	$\mathrm{m^2/s}$
E	energy	J
F	force	N
G	modulus	Pa
H	magnetic field strength	A/m
I	current	A
J_i	flux of state variable a_i	a_i/s
K	magnetic anisotropy	$\mathrm{J/m^3}$
$\mathcal{L}$	Langevin function	–
L	characteristic length	m
L_{ik}	matrix of phenomenological coefficients	–
Le	Lewis number	–
M	magnetization	A/m
N	number of particles	–
N_m	magnetic number, $N_\mathrm{m} = Ra_\mathrm{m}/Ra_\mathrm{g}$	–
Nu	Nusselt number	–
$\mathbf{P}$	vector of nodal pressures	Pa
Pr	Prandtl number	–

Q	quality factor	–
$\mathbf{R}$	residual vector	
Ra_{g}	gravitational Rayleigh number	–
Ra_{m}	magnetic Rayleigh number	–
Re	Reynolds number	–
S	entropy	J/K
S_{T}	Soret coefficient	1/K
$\mathbf{T}$	vector of nodal temperatures	K
T	temperature	K
$\mathbf{T}$	torque vector	Nm
$\mathbf{U}_i$	vector of nodal velocities	m/s
V	volume	m^3
$\mathbf{W}$	weighting function vector	–
X_i	thermodynamic force, gradient of state variable a_i	a_i/m

Small letters

a	scale of a wavelet	$-, \mathrm{s}$
b	location of center of a wavelet	$-, \mathrm{s}$
c_p	specific heat capacity at constant pressure	J/kgK
c_v	specific heat capacity at constant volume	J/kgK
d	diameter	m
$\mathbf{e}$	unit vector	–
f	frequency	$1/\mathrm{s}, \mathrm{Hz}$
g	acceleration of gravity	$\mathrm{m/s}^2$
h	height (thickness)	m
$\mathbf{i}, \mathbf{j}, \mathbf{k}$	unit vectors in x, y and z-directions	–

$\mathbf{j}$	flux vector	m/s
$\mathbf{j}_\mathrm{m}$	magnetic dipole moment	Wbm
k	wave number	1/m
k_B	Boltzmann constant	J/K
m	magnetic moment	Am^2
n	particle number density	$1/\mathrm{m}^3$
p	pressure	Pa
q	heat flux	$\mathrm{W/m}^2$
r	radius	m
r	radial, cylindrical coordinate	–
t	time	s
$\mathbf{u}$	vector of velocity components u, v, w	m/s
u	velocity in x-direction	m/s
v	velocity in y-direction	m/s
w	velocity in z-direction	m/s

Greek letters

α	volume fraction of a component	–
β	coefficient of thermal expansion	1/K
β_m	pyromagnetic coefficient	1/K
χ	differential susceptibility	–
χ_L	Langevin susceptibility	–
δ	thickness of coating	m, nm
ϵ	penalty parameter	–
ϕ	solid volume fraction	–
ϕ	azimuthal angle, cylindrical coordinate	°, rad

ϕ_{m}	magnetic scalar potential	A
γ	strain	–
η	viscosity	kg/ms
φ	interpolation function for velocity	–
κ	thermal diffusivity	m^2/s
λ	molecular length scale	m
λ	thermal conductivity	W/mK
μ_0	vacuum permeability	H/m
μ	permeability	H/m
μ_{r}	relative permeability $\mu_{\mathrm{r}} = \mu/\mu_0$	–
μ_{s}	chemical potential of solute	J/kmol
$\mu\Phi$	viscous dissipation	W/m^3
ν	kinematic viscosity	m^2/s
Ω	rotation rate	$1/\mathrm{s}, \mathrm{Hz}$
ω	solid angle	sr
ω_0	dimensionless frequency	–
θ	(zenith) angle, cylindrical coordinate	$^{\mathrm{o}}, \mathrm{rad}$
ρ	density	kg/m^3
τ	characteristic time	s
τ	stress tensor	N/m^2
τ_{F}	Fourier time period	s, h
ϑ	interpolation function for temperature	–
ξ	Langevin parameter	–
ψ	interpolation function for pressure	–
ψ	wavelet function	–

Subscripts

a	anisotropy
B	Brownian
C	cold
c	carried fluid
cr	critical
D	diffusion
d	domain
eff	effective
ext	external
f	carrier fluid
H	hot
hydro	hydrodynamic
i	i^{th} component of a mixture
L	Langevin
m	magnetic
m	mixture
meso	mesoscopic
mf	magnetic fluid
Mi	diffusion velocity of component i
N	Néel
p	particle
proj	projection
s	saturation
s	slip

S Stokes

T thermal

tot total

Superscripts

D dissipative

R reactive

’ correction term

* guessed value, normalized value

Abbreviations

CCP cubic close packing

CWT continuous wavelet transform

DWT discrete wavelet transform

EAS equi angle skewness

LUT Lappeenranta University of Technology

MEFT modified effective field theory

MEMS micro-electro-magnetic systems

MRI magnetic resonance imaging

PDF probability density function

PSU Perm State University

RCP random close packing

RDF radial distribution function

SIMPLE semi-implicit method for pressure linked equations

1 Introduction

In this thesis the mechanisms and the flow behavior of complex solid-fluid suspensions have been studied theoretically and by numerical simulations. In colloidal suspensions, the interactions between the particles play an important role in the physics of the system. Real colloidal suspensions are practically always polydisperse, which makes the macroscopic description of the problem difficult or impossible. In addition to internal interaction forces between the particles and between the fluid and the particles, there may be external forces, such as gravity or magnetic force, which have a different effect on solid particles and the fluid surrounding them. Most often in the studies of colloidal suspensions the objective is to find a way from the microscopic structure of the system to the realistic description of the macroscopic properties of the fluid, such as density or viscosity.

Despite enormous development in computational power during the past few decades, real natural systems or engineering applications usually cannot be modeled by direct numerical simulations. However, the molecular or particle dynamics and direct numerical simulations are very important tools in the research of complex systems. If the large-scale behavior of some complex system can be captured by means of numerical simulations, we may at least assume that our model describes the physics of the system correctly. One major problem with the microscale simulations is that it is rarely possible to verify the microscopic behavior of the system experimentally.

Perhaps the most famous statement of the limited capability to study a system experimentally is the uncertainty principle of Heisenberg (1927), which claims that *"The more precisely the position is determined, the less precisely the momentum is known in this instant, and vice versa".* Heisenberg also argued that every concept has a meaning only in terms of the experiments used to measure it, and things that cannot be measured really have no meaning in physics. For instance, the path of a particle has no meaning beyond the precision with which it is observed. In light of Heisenberg's theory we should distinguish two different areas of science, namely theoretical physics and the modeling of physical systems. In theoretical physics one tries to create an accurate description of the physical world, and according to Heisenberg, the use of concepts which cannot be observed experimentally has no meaning. On the other hand, in the numerical modeling the aim is to make a model which reproduces the experimentally observed macroscopic behavior of the system in the best possible way, no matter the concepts used in the model. In this thesis the main focus is on the latter approach, although the theoretical background and basic principles are carried alongside the numerical modeling.

The thesis is mainly about the theoretical and numerical study of magnetic fluids and especially about the numerical simulations of thermomagnetic convection. Starting from the first theoretical study of thermomagnetic convection (Finlayson, 1970), in most theoretical and numerical studies the magnetic fluids have been considered as a homogeneous medium. In recent years, the thermodiffusion (Völker and Odenbach, 2005; Shliomis and Smorodin, 2002) and other mechanisms of particle transfer (Blums, 2005) have been taken into consideration. The experiments (Bozhko and Putin, 2003) in part show that at terrestrial conditions, the heat and mass transfer in magnetic colloids are essentially complicated for the most part because of uncontrollable gravitational sedimentation of magnetic particles and their aggregates. Close to the threshold the competitive action of density gradients of a thermal and sedimentation nature results in mostly spatiotemporally chaotic convection with oscillatory and traveling wave regimes. Previously, similar irregular behavior near the convection onset, so-called spatiotemporal chaos, was revealed in gases, binary mixtures and nematic liquid crystals. (Getling, 1998)

In this thesis, the magnetic field control of convection instabilities and heat and mass transfer in magnetic fluids, composed of single domain particles of magnetic material suspended in a liquid carrier, have been investigated. Simulation models based on finite element and finite volume methods have been developed. In addition to standard conservation equations, the magnetic field inside the simulation domain is calculated from Maxwell equations and necessary terms to take into account the magnetic body force and magnetic dissipation have been added to the momentum equation. Numerical simulations of magnetic fluid convection have been carried out for different geometries and magnetic fields and the simulation models have been tested against available experimental results. In order to study the effect of non-homogeneous particle distribution on magnetic fluid convection, the simulations have been carried out by using both single phase and two-phase mixture models.

The main applications of the phenomena investigated here are related to the use of magnetic fluids as a heat transfer medium. Magnetic fluids have been used to enhance the heat transfer, especially in electronic devices, where the presence of a magnetic field or magnetic field gradient causes magnetic convection and an increase in the heat transfer rate. Cooling based on thermomagnetic convection is particularly useful in systems used in low gravity — space applications, where gravitational free convection is absent, or systems in which the natural circulation should occur against the gravity or despite the position of the device. In these passive cooling systems, the long term stability of the fluid is extremely important. Hypothetical, pure and monodisperse magnetic fluid is stable against agglomeration and grav-

itational sedimentation. However, in real magnetic fluids, the interactions between polydisperse particles may lead to unexpected instabilities.

We have also attached two articles, Publications VII and VIII, (Jalali et al., 2002; Zamankhan et al., 1999) about the study of shear flow of dense granular material. The main results of these papers have been published in an earlier doctoral thesis by Jalali (2000) and Zamankhan (2004). The publications are included also in this work despite the fact that the dominant effects in dense granular flows and thermomagnetic convection of magnetic fluid are quite different. The reason for this is that some methods of analysis, presented in (Jalali et al., 2002; Zamankhan et al., 1999) have been adopted for the study of magnetic fluid convection. Furthermore, the comparison of the characteristic parameters of these quite opposite systems gives some general insight about the magnitude and importance of different forces on the behavior of complex fluids.

A major interest and cause of problems in real systems and engineering applications are instabilities, which are difficult to model and predict theoretically. These instabilities are often absent when systems are studied using idealized models. The reason for this is the fact that the instable behavior of a complex system is often caused by the secondary effects, which are neglected in simplified models.

Studying systems with different dominant effects gives a wider perspective to the study of complex systems and it also helps to keep the existence of the secondary forces in mind. In addition, the phenomena, such as intermittency and exponential behavior of the probability distribution, observed in different complex systems are often similar although the dominant effects in the systems may be different. For example, in granular flows the interaction between gravitational compactification and shear induced melting leads to stick-slip motion and normal force peaks an order of magnitude larger than the mean value (Jalali et al., 2002; Zamankhan et al., 1999), Publications VII and VIII. Similarly, the interplay between the gravitational sedimentation of magnetic particles and their aggregates and the magnetic and thermal buoyancy forces leads to oscillatory convection where the magnitude of the convective heat flux varies greatly (Bozhko and Tynjälä, 2005; Bozhko et al., 2004, 2005; Tynjälä et al., 2005), Publications I, II, III and IV.

The thesis has been organized as follows: In Chapter 2, some common methods for the characterization and analysis of complex systems are presented. Chapter 3 is devoted to the presentation of extraordinary behavior, possibilities and properties of magnetic fluids. Chapter 4 gives a brief description of the numerical methods used in the analysis. In Chapter 5, the studied cases are introduced and the presentation and discussion of the results are given for each case separately. Chapter 6 concludes the work, and

in Chapter 7, a brief epilogue is given for readers to keep the realities of the world in mind. Publications related to the thesis are attached as appendices I to VIII.

2 Characterization of suspensions

In order to characterize either quantitatively or qualitatively the behavior of complex systems some tools are needed. There are many ways how we can bring order to complex systems. In next few chapters, some of the most common methods and definitions, used in the studies of complex systems, from characteristic parameters through thermodynamics and statistical mechanics to rheology of complex materials and analysis of complex systems, will be presented.

2.1 Parameters characterizing suspensions

The brevity of different solid-fluid suspensions is large and practically all environmental systems can be considered as suspensions of different substances or different phases of a pure substance. In this thesis, the focus is on multicomponent flows consisting of solid particles suspended in a carrier fluid, special cases being dense granular flows and dilute magnetic fluids. In Table 2.1 examples of typical particle sizes of different type of solid-liquid-gas dispersoids are presented.(Lapple, 1961)

Table 2.1: Particle diameters of typical particles and particle dispersoids. Table is modified based on the original work of Lapple (1961).

	Particle diameter (μm)							
	0.0001	0.001	0.01	0.1	1	10	100	1000 (1 mm)
Technical definitions	*Solids:*		← Fume →		←	Dust →		
	Liquids:		← Mist →			← Spray →		
	Soil:		← Clay →		← Silt →	← Fi ne sand →	← Coarse sand →	Gravel →
Common atmospheric dipersoids			← Smog →		← Clouds and fog →	→ Mist ←		Rain →
						→ Drizzle		←
Typical particles and gas dispersoids	Gas molecules →		← Oil smokes →		←	Fly ash →		
		← Viruses →			← Bacteria →	← Hair →		
		Magnetic			←	Pulverized coal →		
		← **fluid** →			← Coal dust →	← **Granular materials** →		
		particles						

Main parameters used to describe the properties of suspensions are the size, the shape and the solid volume fraction of the particles, particle distributions and the viscosity of the carrier fluid. Based on these basic parameters and on the other properties of the system under consideration, order of magnitude estimates of the forces present in the system may be conducted.

Characteristic parameters of systems presented in this thesis vary greatly. Dense granular flows consist of rather large particles from about one hundred microns to few millimeters, the solid volume fraction is high and the effect of carrier fluid, a gas of low viscosity, has been neglected. On the other end, magnetic fluids consist of nanosized particles, with low solid volume fraction and often quite viscous carrier liquid. In granular flows the flow dynamics is mainly governed by the particle collisions and the effect of carrier fluid is neglected whether in magnetic fluids the interparticle collisions are often neglected. Moreover, the size of the magnetic fluid particles is so small that they are considerably affected by the Brownian motion and most often in the previous studies magnetic fluids have been considered stable against gravitational sedimentation.

2.1.1 Size and shape of the particles

Size of the particles is a main parameter, when the properties of a suspension are considered. Particle size is usually compared to the molecular size λ. As presented in Table 2.1, size of a gas molecule is about $\lambda \approx 10^{-10}$ m = 1 Å (Ångström). For suspensions, in which the particle diameter $d_p \gg \lambda$, the effect of Brownian motion due to collisions of carrier fluid molecules is often negligible. On contrary, in colloidal suspensions the particle diameters are typically from 10 ... 20 nm (Raikher and Rusakov, 2003), the particle movement is strongly influenced by the Brownian motion.

Shape of the particle has an effect especially on drag force and slip velocity between the fluid and the particles. Usually it is impossible to use real particle shapes in the calculations and the particles are modelled using well defined basic geometry, such as spheres, disks or rods. When translational drag force is considered, the key parameter is the face projection area A_{proj} against the flow.

Particle Reynolds number, defined as

$$Re_{\mathrm{p}} = \frac{\rho_{\mathrm{f}} d_{\mathrm{p}} u_{\mathrm{s}}}{\eta_{\mathrm{f}}}, \tag{2.1}$$

where ρ_{f} is the density of the carrier fluid, d_{p} is the particle diameter, u_{s} is the slip velocity between the particles and the fluid and η_{f} is the viscosity of the carrier fluid. Particle Reynolds number is often defined based on hydraulic diameter of the particles. For small particles, when the particle Reynolds number $Re_{\mathrm{p}} < 1$, which is the case with magnetic fluids, Stokes drag coefficient $C_{\mathrm{D,S}} = 24/Re_{\mathrm{p}}$ may be applied and the drag force F_{D} may be calculated using the Stokes drag law defined as

$$F_{\mathrm{D,S}} = C_{\mathrm{D,S}} \frac{\rho u_{\mathrm{s}}^2}{2} A_{\mathrm{proj}} = 3\pi\eta_{\mathrm{f}} d_{\mathrm{p}}. \tag{2.2}$$

For larger Reynolds numbers, drag coefficient proposed by Schiller and Naumann (Fluent, 2005) equation (2.3), may be used.

$$C_{\mathrm{D}} = \begin{cases} 1 + 0.15Re^{0.687} & , Re_{\mathrm{p}} \leq 1000 \\ 0.0183Re & , Re_{\mathrm{p}} > 1000 \end{cases} \tag{2.3}$$

2.1.2 Solid volume fraction and particle distributions

Solid volume fraction ϕ is another important parameter used to characterize suspensions. Solid volume fraction may be used to evaluate the importance of particle interactions. For dilute suspensions interactions between the particles and particle aggregates are often neglected. To evaluate suspension viscosity of dilute suspensions consisting of smooth spherical particles suspended in fluid of viscosity η_{f} Equation (2.4) first proposed by Einstein (1906) may be used.

$$\eta = \eta_{\mathrm{f}} \left(1 + \frac{5}{2}\phi\right) \tag{2.4}$$

In dense suspensions the dynamics are often collision dominated. Upper limit for the solid volume fraction of system composed of monodisperse spherical particles $\phi_{\mathrm{CCP}} \approx 0.74$ for cubic close packing (CCP) and $\phi_{\mathrm{RCP}} \approx 0.64$ for random close packing (RCP) (Jaeger and Nagel, 1992; Torquato et al., 2000).

The real suspensions are collection of particles of different sizes and shapes, often not evenly distributed. Several different distributions are needed, when the microstructure of the multicomponent systems are evaluated and modeled. In addition to particle size and shape distributions, microstructural correlation functions, such as n-point probability function or radial distribution function (RDF), may be used to describe the microstructure of suspension. RDF shows the average probability of finding the center of a particle at a distance r from the center of a sample particle, as shown in Figure 2.1 (a). Each microstructure has a certain pattern for RDF and it can be considered as a fingerprint of the microstructure. Figure 2.1 (b) shows RDF's for sheared dense granular flow (Zamankhan et al., 1999), Publication VIII, for different solid volume fractions. Peaks on the radial distribution function reveal the presence of ordered phase in the simulations conducted for higher shear rate.

1-point probability function gives probability that randomly placed point is in one phase of a suspension, which for a fluid-solid mixture, such as

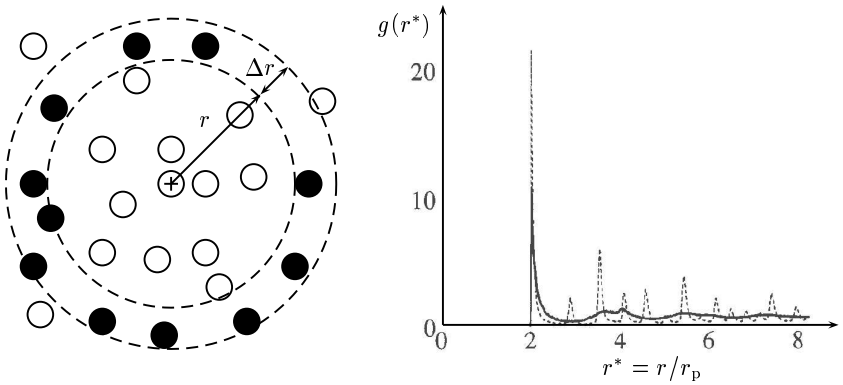

(a) (b)

Figure 2.1: (a) Definition principle of radial distribution function and (b) RDF's $g(r^*)$ obtained from the simulations of shearing of dense granular flows with solid volume fractions $\phi = 0.6$ (dashed line) and $\phi = 0.565$ (solid line), as a function of distance r^*, normalized with the particle diameter, from the particle center. For lower solid volume fraction there is no indication of the crystalline structure, shown by the peaks in the RDF. (Zamankhan et al., 1999), Publication VIII

magnetic fluid or granular material, corresponds to the solid volume fraction. 2-, 3- or n-point probability function gives corresponding probability that the end points of line, triangle or n corners of polygon are in certain phase. Figure 2.2 shows two cases of homogeneous media from which the other one is isotropic and the other one anisotropic. Anisotropy can be detected using n-point probability distribution function. By the definition, the n-point probability function of statistically homogeneous media is space invariant. For statistically isotropic media the n-point probability function is in addition rotationally invariant. (Torquato, 2002)

2.2 Rheology of complex fluids

By the definition, fluids are incapable to resist shearing motion and while deformed they will flow and all shearing energy is dissipated into heat. In the other end, solid materials can be described by their elasticity. When a solid material is deformed, it will store the energy and fight back. When multi-component flows are considered, it is not so clear, whether the material is in fluid or solid phase. They can sometimes behave like a solid, sometimes like a fluid, and sometimes can have features of both phases. (Jalali, 2000)

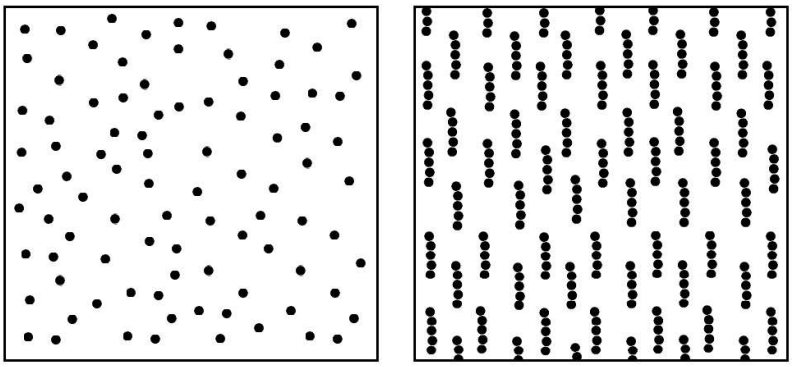

Figure 2.2: (a) Homogeneous and isotropic particle distribution and (b) homogeneous but anisotropic distribution of particles.

In magnetic fluids, there is a two-way interaction between the rheological properties and the microstructure of the fluid. Effective viscosity of the fluid depends on formation of aggregates in the fluid, and on the other hand, the motion of the fluid influences the structure of the aggregates. For magnetic fluid in an applied field, chains containing several particles are the favored form of the aggregates. (Mekhonoshin and Lange, 2004) Other forms are drop aggregates, which may contain thousands of particles (Blums et al., 1989; Gluhov and Putin, 1999). Magnetic fluid in an applied field may form chains and often resembles anisotropic system, such as shown in Figure 2.2 (b).

Memory effect, the dependance of the behavior of a system from the prehistory, is characteristic for viscoelastic systems. Similarly, the experimentally and numerically observed heat flux in magnetic fluid convection is strongly dependent of the prehistory of the experiments (Bozhko and Putin, 2003; Tynjälä et al., 2005), Publication I. The depth of hysteresis loop, shown in Figure 5.4, depends on prehistory of the experiment and is wider for initially non-mixed fluid that for convection mixed fluid, which testifies the presence and shear induced breaking of the aggregates, in the fluid. Shear induced melting has been observed also in charged colloidal suspensions (Ackerson and Clark, 1981) and in dense granular flows (Jalali et al., 2002), Publication VII.

Figure 2.3 shows partial melting of granular material in shear flow experiments (Jalali et al., 2005). The granular material used in this study were spherical steel ball bearings with diameter of 3 mm. Photos are made as a superposition of subsequent video frames. At the rotation rate $\Omega = 0.3$ Hz in Figure 2.3 (a) the sheared layer thickness is approximately 15 mm and the

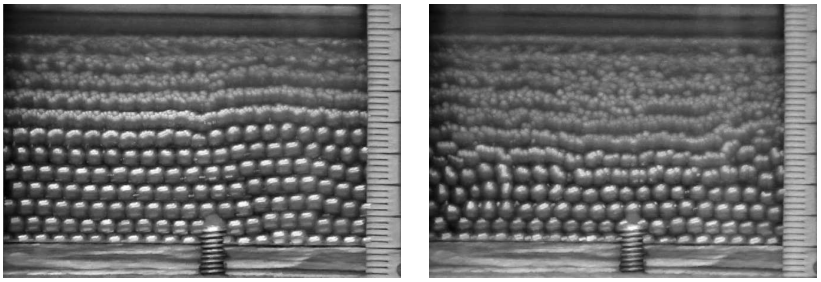

(a) (b)

Figure 2.3: Demonstration of partial shearing in granular shear flow experiment. Monodisperse steel balls (3 mm) under shear flow appear blurred and the rest are still with intermittent small motions. The rotation rates are (a) $\Omega = 0.3$ Hz and (b) $\Omega = 0.5$ Hz. Photos by J. Ritvanen, LUT.

remaining particle layers are almost still. At rotation rate $\Omega = 0.5$ Hz, shown in Figure 2.3 (b), the layer thickness has increased to almost 25 mm. Presence and melting of similar ordered solid and quasifluid phases were observed also in numerical simulations (Jalali et al., 2002), Publication VII.

One way to describe complex material properties is by the theory of viscoelasticity. Viscoelastic materials are intermediate between elastic solids and viscous fluids and neither elasticity nor viscosity is enough to characterize them. A viscoelastic material is intermediate and stores some energy and flows a little when deformed.

For a newtonian fluid the stress tensor τ is symmetric and it may be presented with help of a single coefficient of viscosity as

$$\tau_{\mathrm{f}} = \eta \frac{d\gamma}{dt} \tag{2.5}$$

For completely elastic material the stress would be

$$\tau_{\mathrm{e}} = G\gamma \tag{2.6}$$

In viscoelastic case the stress is combination of these two effects. There exist several phenomenological models to represent this relationship for different viscoelastic materials. Two most common models are Maxwell model and Kelvin model. In Maxwell model (2.7) the stress is constant through the system and the total strain is the sum of elastic and viscous strain components. According to Kelvin model (2.8) the total stress is a sum of viscous and elastic stress terms and the strain is equal through the system (Creus, 1986).

$$\tau_{\mathrm{tot}} = \tau_{\mathrm{f}} = \tau_{\mathrm{e}} = \tau \qquad \frac{d\gamma_{\mathrm{tot}}}{dt} = \frac{d\gamma_{\mathrm{f}}}{dt} + \frac{d\gamma_{\mathrm{e}}}{dt} = \frac{1}{G}\left(\frac{d\tau}{dt} + \frac{\tau}{\eta}\right) \tag{2.7}$$

$$\gamma_{\mathrm{tot}} = \gamma_{\mathrm{f}} = \gamma_{\mathrm{e}} = \gamma \qquad \tau_{\mathrm{tot}} = \tau_{\mathrm{f}} + \tau_{\mathrm{e}} = \eta\frac{d\gamma}{dt} + G\gamma \tag{2.8}$$

In addition to macroscopic phenomenological models like Kelvin or Maxwell model, there are several other ways to consider the viscoelastic properties of a complex fluid. In molecular dynamics and particle dynamics simulations the interactions between particles are modelled directly. For example, in modified hard sphere algorithm for granular flows (Zamankhan et al., 1999), (Jalali et al., 2002) the energy dissipation in viscoelastic binary collisions of particles was taken into account using the normal and tangential coefficients of restitution.

2.3 Analysis of complex systems

Standard method in signal analysis, Fourier analysis, gives information about the dominant frequencies present in the system, but loses information about the time localization of the oscillations. Windowed Fourier transform or wavelet transform can be used to analyze frequency content of a time-dependent signal locally in time (Daubechies, 1990).

In granular flows, zones where particles form solid-like crystal structures, and zones where particles flow like a fluid, may coexist in equilibrium or vary both temporally and spatially. (Jalali, 2000; Jalali et al., 2002) Similarly temperature oscillations observed in the experiments and numerical simulations of magnetic fluid convection, revealed spatiotemporal chaotic fluctuations, composed of high and low-frequency content, Publications I, III and IV (Tynjälä et al., 2005; Bozhko et al., 2004, 2005).

In order to study the nature of spatiotemporal variations present in studied complex systems, wavelet analysis was used. Wavelet analysis gives information in the phase-scale level and may be used to track the changes in the convection patterns as a function of time. There exists two types of wavelet transforms, continuous (CWT) and discrete (DWT). The wavelet transform of a function $f(t)$ using the wavelet ψ, is defined as (Farge, 1992)

$$C(a,b) = \frac{1}{\sqrt{a}}\int f(t)\psi\left(\frac{t-b}{a}\right)dt, \tag{2.9}$$

where parameters a is wavelet scale for dilation and b is the location of center of wavelet for translation. For CWT parameters a and b are real numbers

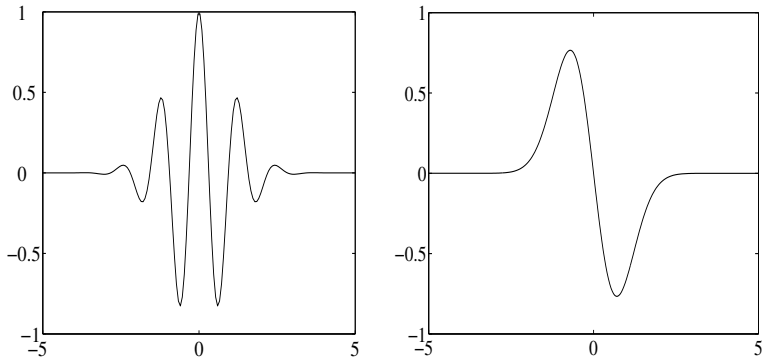

Figure 2.4: (a) Morlet wavelet, (b) Gaussian wavelet

and vary continuously (Jalali et al., 2002). The mathematical formulation of Morlet wavelet, shown in figure 2.4 (a), is

$$\psi\left(\frac{t-b}{a}\right) = \pi^{-\frac{1}{4}} e^{i\omega_0\left(\frac{t-b}{a}\right)} e^{-\frac{1}{2}\left(\frac{t-b}{a}\right)^2}, \tag{2.10}$$

where non-dimensional frequency ω_0 is taken to be 5 in this study. Morlet wavelet is complex, oscillating and thin in Fourier space, which makes it a powerful tool for detecting frequency content of an oscillating signal (Vecsey, 2002). In fluid mechanics and turbulence applications complex Morlet wavelet is mostly used (Sikiö, 2004). Gaussian wavelets, like one shown in Figure 2.4 (b), on the other hand are more suitable for detection of the structure and behavior of multi-dimensional and geophysical fields such as gravity or temperature fields (Vecsey, 2002).

When continuous wavelet transform (CWT) is used, the relationship between the time period used in Fourier analysis τ_{F} and corresponding wavelet scale a is always linear and for Morlet wavelet the relationship is (Vecsey, 2002)

$$\tau_{\mathrm{F}} = \frac{4\pi a}{\omega_0 + \sqrt{2+\omega_o^2}}. \tag{2.11}$$

In Figure 2.5 (a) a signal composed of five sinusoidal harmonics, corresponding to time periods of 4 h, 2h, 1 h, 30 min and 10 min. Figures 2.5 (b) and (c) present the wavelet analysis of the given signal using (b) complex Gaussian and (c) complex Morlet wavelets. Gaussian wavelet is able to detect peaks in sinus signal but the frequency resolution is not as good as with Morlet wavelet.

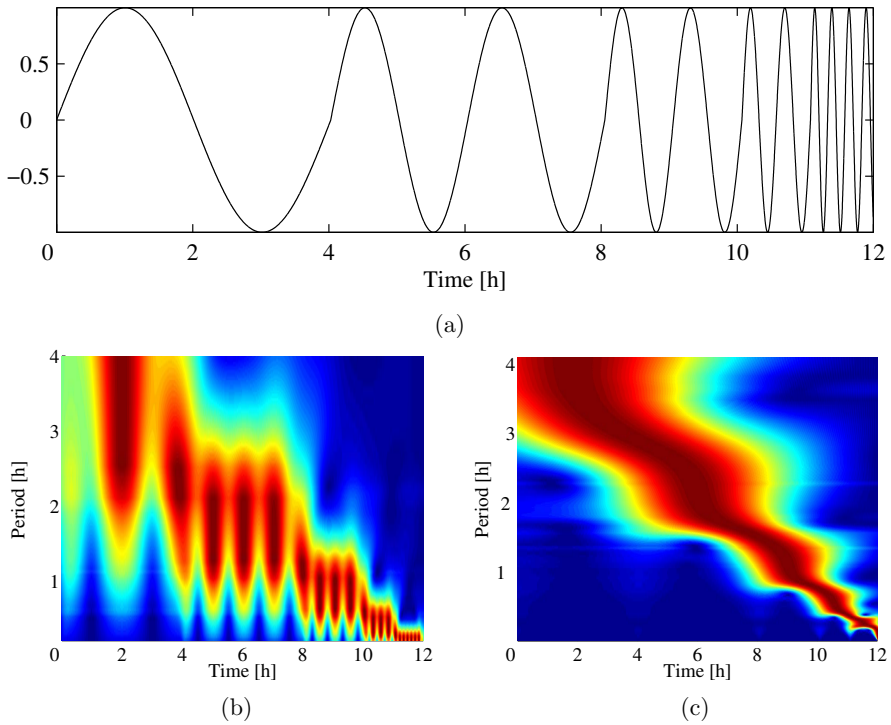

Figure 2.5: (a) Signal composed of five sinusoidal harmonics, corresponding to time periods of 4 h, 2h, 1 h, 30 min and 10 min, (b) and (c) present the wavelet analysis of the given signal using (b) complex Gaussian and (c) complex Morlet wavelets.

Besides Fourier and wavelet analysis probability density functions (PDF) are frequently used in the studies of complex systems. PDF's are used to study the fluctuations and distribution of fluctuations around the mean value. While PDF of a random signal is typically Gaussian, exponential behavior is characteristic for chaotic and turbulent systems, where improbable events are much more likely than with the Gaussian form. Gaussian estimates, formed by short time series will give an entirely incorrect picture of large-scale fluctuations of the system (Goldenfeld and Kadanoff, 1999).

Simulations of dense granular flows (Zamankhan et al., 1999; Jalali et al., 2002) revealed the presence of an exponential behavior of the PDF in the normal stress signals exerted on the moving wall, as shown in Figure 2.6 (See also Publications VII and VIII), typical for chaotic systems. The model predicted peaks in the normal stress signal whose largest values are about five times the average value of the normal stress.

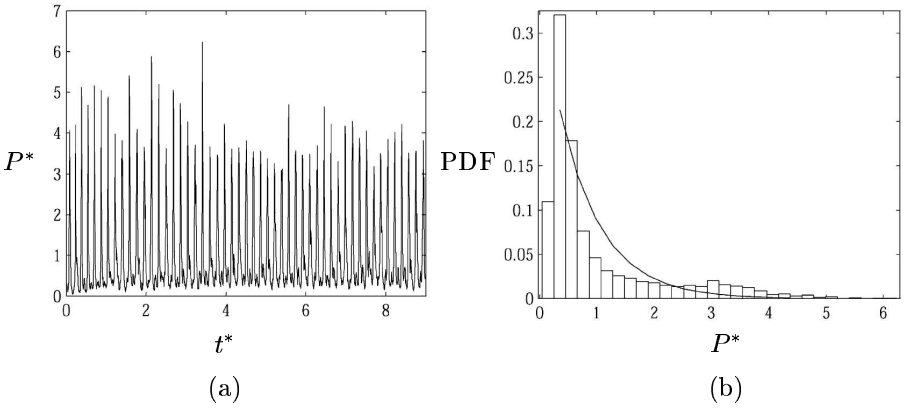

Figure 2.6: (a) The dimensionless normal stress P^* measured on the fixed bottom wall as a function of dimensionless time t^*, and (b) the PDF of the dimensionless normal stress. The solid line in the right figure represents an exponential fit to the PDF. (Jalali et al., 2002)

2.4 Thermodynamical considerations

The requirement for any system is the consistency with the laws of the thermodynamics. In other words, the conservation of energy and tendency to equilibrium state by maximizing the system entropy. Strictly speaking classical thermodynamics is concerned only with equilibrium processes (Lee et al., 1973). Theory of non-equilibrium thermodynamics or thermodynamics of irreversible processes are often needed to take into account the irreversibilities, such as heat conduction, diffusion or viscous flow, of the system (de Groot, 1951).

2.4.1 Statistical mechanics

In the classical thermodynamics the general laws governing the transfer of energy between macroscopic systems are considered. Another approach to thermodynamics is through the atomic theory of matter, considering positions and velocities of single atoms or molecules. Statistical methods is then used to predict the properties of the macroscopic systems based on properties of microsystems. Statistical thermodynamics creates a link between coordinates of statistical mechanics and those of classical thermodynamics.(Lee et al., 1973)

Kinetic theory is often linked to statistical thermodynamics. As in classical thermodynamics slow processes between equilibrium states, quasistatic, are

considered, the kinetic theory is often needed to give the velocity with which the equilibrium is reached.

Ludwig Boltzmann presented a statistical measure of the probability of certain configuration of nuclei or electrons in a system. In statistical mechanics the entropy S is defined by the Boltzmann relation (2.12), which relates the entropy of the system to the possible states of systems of equal energy $\Omega(E)$ through Boltzmann constant k_{B},

$$S = k_{\mathrm{B}}\Omega(E). \tag{2.12}$$

If a system with constant volume V and total energy E is considered, by the definition, the temperature of the system is $T = \partial E/\partial S$ and heat capacity $\partial E/\partial T$. It can be shown, see e.g. (Kubo, 1965), that the probability of quantum state l of the system $f(l)$ is proportional to the energy of the quantum state E_l and thermal energy of the system $k_{\mathrm{B}}T$, according to canonical distribution, shown in Equation (2.13).

$$f(l) \propto \exp \frac{-E_l}{k_{\mathrm{B}}T}, \tag{2.13}$$

2.4.2 Thermodynamics of irreversible processes

In the studies of magnetic fluids many irreversible processes exists. These processes may be formulated with the help of fluxes and thermodynamic forces. Common examples of theses fluxes and forces are e.g. heat flux caused by the temperature gradient, mass flux due to concentration gradient and shear stress due to velocity gradient. These effects may also occur simultaneously giving rise to new effects.

Central theory in the study of fluxes caused by thermodynamic forces are the Onsager reciprocal relations (Onsager, 1931a,b; de Groot, 1951). Onsager's fundamental theory states that if a proper choice is made for fluxes J_i and thermodynamic forces X_i the matrix of phenomenological coefficients L_{ik} is symmetric

$$L_{ik} = L_{ki}, (i, k = 1, 2, \ldots, n). \tag{2.14}$$

Diagonal elements of matrix L_{ii} represent e.g. coefficients of heat conductivity, diffusion and viscosity.

Entropy production, a positive definit function, in a binary mixture depends on three thermodynamic forces, namely gradients of temperature, velocity and solute chemical potential, $\dot{S} = f(\nabla_i T, v_{ij}, \nabla_i \mu_s)$. In the presence of magnetic field, the components of induction field $\mathbf{B}$, must be included as independent variables (Müller and Liu, 2001). Thermodynamic forces and

Table 2.2: Thermodynamic forces and fluxes present in systems of binary magnetic fluids

Flux	**Thermodynamic force**			
	$\nabla_i T$	v_{ij}	$\nabla_i \mu_\mathrm{s}$	$\nabla B_i(H_i)$
Heat	thermal conduction, λ	thermo-elasticity	Dufourt effect, D_T	magnetocaloric effect
Momentum	thermal expansion	viscous flow, elasticity, η, G	precipitate consolidation	Kelvin force magnetodissipation
Mass	thermal diffusion, D_T	dissolution precipitation	ordinary diffusion, D	magneto-phoresis
Magnetization	pyromagnetic effect	deformation, reorientation	magnetic phase fraction	magnetic induction, μ

fluxes present in binary magnetic fluids are presented in Table 2.2. (Bird et al., 1960)

Hydrodynamics of isotropic, single component magnetic fluids in the presence of magnetic field were recently studied by Müller and Liu (2001). Binary mixtures were studied in the absence (Ryskin et al., 2003) and in the presence (Ryskin and Pleiner, 2004) of magnetic field. Important cross-phenomena in the study of magnetic convection is thermal diffusion or Soret effect, the flux of particles due to the temperature gradient. As in pioneering work of Finlayson (1970), in most theoretical studies the magnetic fluids have been considered as homogeneous medium. Last years, the thermodiffusion mechanism of particle transfer has been taken into consideration (Shliomis and Smorodin, 2002). In many cases the Soret effect indeed is negligible, because the relaxation time for the mass diffusion can be considered infinite compared to the time scale for the heat conduction. Following the same reasoning the relaxation time for magnetic fluid magnetization, discussed more detailed in Section 3.2.1, may be considered infinite fast compared to the time scale of convective motion, and the magnetoviscous effects originating from the difference between particle magnetic moments $\mathbf{m}$ and applied field $\mathbf{H}$ are negligible. As stated by the Onsager relations, these cross-phenomena are reciprocal in the sense that a counter phenomena exists. For example the cross-phenomena for Soret effect, the flux of particles due to temperature gradient, is so called Dufourt effect, the heat flux due to gradient in solute chemical potential. However, the Dufourt effect is often neglected being important only in gas suspensions Ryskin et al. (2003).

3 Magnetic fluids

> *It may be said that among the known disperse systems, only in magnetic fluids does the dispersed phase represent an active element transmitting the acting forces to the entire system as a whole.* (Fertman, 1990)

Magnetic fluids are relatively new area of science. Initially in the 1960's the magnetic fluids were studied for a system, which could convert heat to work with no mechanical parts (Rosensweig, 1997).

Magnetic fluids are colloidal dispersions of single domain particles of magnetic material - iron, cobalt, magnetite suspended in liquid carrier, such as kerosene or water. In order to prevent the coagulation, particles are coated with surface-active material, either long chained molecules such as in Figure 3.1, or by an electro-static layer. In the absence of magnetic field the fluid behaves as a normal single component fluid. When an external magnetic field is applied, the fluid is magnetized, and the apparent fluid properties, such as density or viscosity, may be changed. The change of apparent viscosity is related to the coupling of the microscopic particle rotation to the macroscopic vorticity of the flow. In a static magnetic field the magnetic torque prevents particles from rotating and thus causes an extra viscous dissipation in the carrier liquid, which leads to an enhanced effective viscosity, the so called rotational viscosity (McTague, 1969). Later Shliomis and Morozov (1994) postulated that the change of effective viscosity may also be negative. Negative viscosity effect in magnetic fluids was first time proven experimentally by Bacri. et al. (1995). Negative viscosity can be understood as a transformation of energy of alternating magnetic field into kinetic energy of magnetic particles. Rotating magnetic particles act like a nanosized motors and actively reduce the friction between neighboring fluid layers (Zeuner et al., 1998).

Since their invention, when the unique properties of magnetic fluids were discovered, several applications for magnetic fluids have been considered. The variety of applications is diverse ranging from, technical and biomedical to scientific applications. Some of the possible applications are listed in Table 3.1.

Magnetic fluids have been used to enhance the heat transfer, especially in electronic devices, where the presence of magnetic field or magnetic field gradient causes magnetic convection and an increase in the heat transfer rate. Cooling based on thermomagnetic convection is particulary useful in systems used in low gravity — space applications, where gravitational free convection is absent, or systems in which the natural circulation should oc-

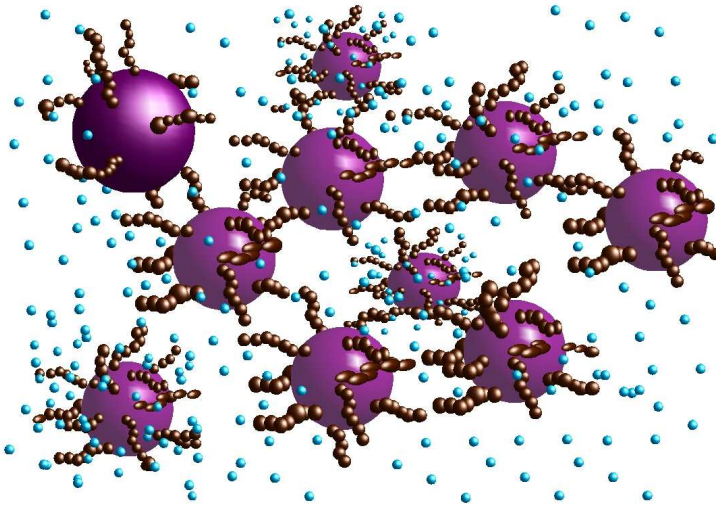

Figure 3.1: Artistic view of a magnetic fluid. Single domain ferromagnetic particles are coated with long chained molecules to prevent particle agglomeration and suspended in an appropriate carrier fluid.

cur against the gravity or despite the position of the device. In these passive cooling systems, the long term stability of the fluid is extremely important. Hypothetical, pure and monodisperse magnetic fluid is stable against agglomeration and gravitational sedimentation. However, in real magnetic fluids, the interactions between polydisperse particles often leads to formation of aggregates and consequently to unexpected instabilities, which may cause system failure. Magnetic fluids have also been considered for an absorbent and heat transfer media for solar collectors (Pode and Minea, 2000).

Another field, where the results and methods used in this thesis may be applied, is the use of magnetic fluid as a controllable model fluid to study basic physical phenomena. For example, magnetic fluids have been used to simulate spherical mantle convection by creating a central gravity conditions using magnetic field (Rosensweig et al., 1999). Magnetic fluid offers also a new magnetic field controllable system for the study of so-called spatiotemporal chaos (Getling, 1998) or crystal growth from paramagnetic melts. Besides magnetic fluids (Bozhko and Putin, 2003; Bozhko et al., 2004), the irregular behavior near the convection threshold have been studied experimentally, for instance by Morris et al. (1996) spiral-defect chaos in gases, Fauve and Laroch (1984) irregular oscillations in mercury, Bestehorn et al. (1980) travelling waves in binary mixture, Dennin et al. (1996) chaotic localized states

Table 3.1: Examples of technical, biomedical and scientific applications of magnetic fluids

Technical Applications	**Biomedical Applications**	**Scientific Applications**
Heat transfer medium	Drug delivery	Controllable model fluid
Damping, sealing	Hyperthermia	Mantle convection
Separation processes	Contrast agent for magnetic	Spatiotemporal chaos
Sensors, actuators etc.	resonance imaging (MRI)	Crystal growth in
Nanotechnology, micro-electro-		paramagnetic melts
mechanical systems (MEMS)		

in nematic liquid crystal and Daniels et al. (2000) in an inclined layer of low Prandtl fluid and Assenheimer and Steinberg (2000) target states in SF_6 close to its gas-liquid critical point.

One of the most exciting property of magnetic fluids is the possibility to control properties, like apparent density or viscosity, by external magnetic field. The possibility of magnetic fluid control gave rise to the development of numerous technical applications, such as a liquid O-ring in rotary and exclusion seals, as dampers in stepper motors and shock absorbers (Berkovsky et al., 1993). The fact that the apparent density of magnetic fluid can be increased by applying a magnetic field creates the ability to separate objects of different density through floatation or sinking. Magnetic fluids have been used for years in material separation processes in the mining industries, although so far with limited economic advantage.

Perhaps most likely an average consumer finds magnetic fluids from his home electronic devices. Magnetic fluids have been used to dampen the vibrations in consumer audio loudspeakers (Berkovsky et al., 1993). This form of damping is very reliable as the viscosity and retention capability of the fluid can be easily controlled to meet device requirements. In addition to the damping benefits in audio loudspeakers, magnetic fluid also provides an efficient heat transfer medium to conduct heat away from the coil. Also almost every computer disk drive uses magnetic fluid rotary seal for contaminant exclusion and the semiconductor industry uses silicon crystal growing furnaces that employ magnetic fluid rotary shaft seals (Zahn, 2001).

Magnetic liquids can also be used for drag reduction in pipelines where magnets position the fluid to form a coating of the pipe wall such that high-viscosity liquids can 'float' on the magnetic liquid layer. Further promising fields for the future applications can be found from medical science, biotechnology, and nanotechnology.

3.1 Physical properties of magnetic fluids

Magnetic fluids are suspensions of nanoscale magnetic particles in appropriate carrier liquid, which are sensitive to external magnetic field. (Rosensweig, 1997) To avoid agglomeration due to attractive dipole-dipole or Van der Waals forces, each particle is coated by long-chain molecules or by an electrostatic layer. Due to the smallness of the particles the properties of magnetic fluids are substantially affected by thermal Brownian motion.

Real magnetic fluids are colloids with varying particle size and shape. In addition to the non-homogeneity the properties of the fluid are strongly dependent on the applied magnetic field and when non-isothermal systems are considered on the temperature. Correct formulation of the physical properties of such complex systems is essential when the ferrohydrodynamic systems are considered.

Density ρ and the specific heat c_p of the magnetic fluid (mf) may be calculated under the assumption of additivity employing the known coefficients of particles (p) and that of carrier fluid (f).

$$\rho_{\mathrm{mf}} = \phi\rho_{\mathrm{p}} + (1-\phi)\rho_{\mathrm{f}} \tag{3.1}$$

$$c_{p,\mathrm{mf}} = \phi c_{p,\mathrm{p}} + (1-\phi)c_{p,\mathrm{f}} \tag{3.2}$$

In 3.1 and 3.2 ϕ represents the solid volume fraction of magnetic particles.

Maxwell (1881) was first to calculate the effective thermal conductivity λ_{eff} of a composite materials, consisting of a continuous isotropic phase of conductivity λ_{f} containing a random spatial distribution of uniformly-sized spherical inclusions of isotropic conductivity λ_{p}. (Zuzovsky and Brenner, 1977) Maxwell's result for a dilute system may be stated as

$$\frac{\lambda_{\mathrm{eff}}}{\lambda_{\mathrm{f}}} = \frac{\frac{\lambda_{\mathrm{p}}}{\lambda_{\mathrm{f}}} + 2 + 2\phi\left(\frac{\lambda_{\mathrm{p}}}{\lambda_{\mathrm{f}}} - 1\right)}{\frac{\lambda_{\mathrm{p}}}{\lambda_{\mathrm{f}}} + 2 - \phi\left(\frac{\lambda_{\mathrm{p}}}{\lambda_{\mathrm{f}}} - 1\right)} \tag{3.3}$$

For small solid volume fractions Maxwell's result may be used to approximate the effective thermal conductivity of a magnetic fluid. For dispersions of non-spherical particles or if the aggregate formation takes place, the thermal conductivity depends on magnetic field. (Blums, 2002)

Viscosity of magnetic fluid is a function of solid volume fraction, applied magnetic field, and shear rate. In the absence of field, the first approximation for the viscosity of magnetic fluid can be calculated with Einstein relation (Einstein, 1906), Equation (2.4) for suspensions with spherical smooth

particles. Better estimate for magnetic fluid viscosity can be calculated from Equation (3.4)

$$\frac{\eta - \eta_0}{\phi\eta} = \frac{5}{2}\left(1 + \frac{\delta}{r}\right)^3 - \left(\frac{5/2\phi_{\mathrm{CCP}} - 1}{\phi_{\mathrm{CCP}}^2}\right)\left(1 + \frac{\delta}{r}\right)^6 \phi, \tag{3.4}$$

where η and η_0 are magnetic and carrier fluid viscosities, ϕ is solid volume fraction, δ and r thickness of coating and radius of particles and $\phi_{\mathrm{CCP}} = 0.74$ corresponds to cubic close packing of spheres (Rosensweig, 1997). In the presence of uniform field, magnetic fluid may be considered as a shear thinning medium. In other words the viscosity of a magnetic fluid decreases when the shear rate increases. The shear thinning is related to the breaking up of particle chains formed in the presence of magnetic field as described in Chapter 2.2.

3.2 Magnetic fluid magnetization

Magnetic fluid behaves like a paramagnetic material. In the absence of field, owing to the Brownian motion, the magnetic moments of particles are randomly orientated and the fluid has no net magnetization. When an external magnetic field is applied, the magnetic moments align along the magnetic field lines generating net magnetization to the fluid. Paramagnetic behavior of magnetic fluid is represented in Figure 3.2.

Net magnetization of a magnetic fluid is a function of the volume fraction of magnetic particles, the temperature of the fluid and the magnitude of the applied field.

Torque acting on small volume δV of magnetically polarized matter in a uniform applied magnetic field $\mathbf{H}_0$.

$$\delta\mathbf{T} = \mu_0\mathbf{M} \times \mathbf{H}_0\delta V \tag{3.5}$$

By definition the magnetic dipole moment $\mathbf{j}_{\mathrm{m}} = \mu_0\mathbf{m} = \mu_0\mathbf{M}\delta V$ [Wbm], where $\mathbf{m} = \mathbf{M}\delta V$ [Am^2] is particle magnetic moment and $\mathbf{M}$ [A/m] is the magnetization. The magnitude of torque T acting on particle whose magnetization vector makes an angle θ with the applied field $\mathbf{H}_0$ is

$$T = j_{\mathrm{m}}H_0 \sin\theta \tag{3.6}$$

Energy expended in rotating the particle from parallel ($\theta = 0$) alignment

$$E = \int_0^\theta T d\theta = j_{\mathrm{m}}H_0 \int_0^\theta \sin\theta d\theta = j_{\mathrm{m}}H_0(1 - \cos\theta) \tag{3.7}$$

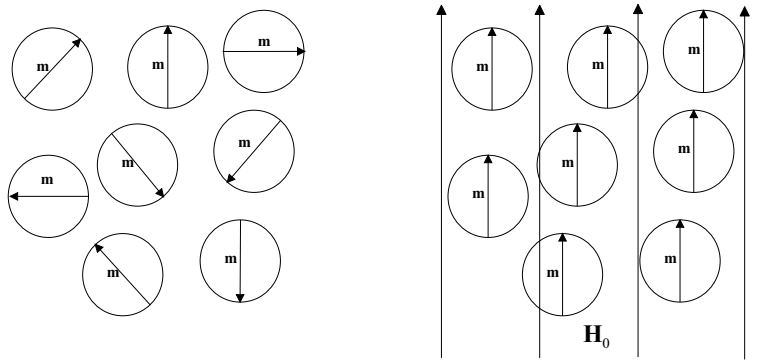

Figure 3.2: (a) In the absence of magnetic field magnetic moments of particles are randomly orientated. (b) When an external magnetic field $\mathbf{H}_0$ is applied the magnetic moments of particles align along magnetic field lines generating net magnetization to the fluid.

Following the classical expressions of the theories of statistical mechanics, see Section 2.4.1, the probability that the direction of magnetic moment $\mathbf{j}_\mathrm{m}$ is in a solid angle element $d\omega$ is given by canonical distribution,

$$f(\theta)d\omega = Ce^{-E/k_\mathrm{b}T}d\omega = C_1 e^{(-j_\mathrm{m}H + j_\mathrm{m}H\cos\theta)/k_\mathrm{B}T}d\omega = C_2 e^{j_\mathrm{m}H\cos\theta/k_\mathrm{B}T}d\omega \tag{3.8}$$

,where $C_2 = C_1 e^{-j_\mathrm{m}H/k_\mathrm{B}T}$, k_B is the Boltzmann constant and T absolute temperature. Value for the proportionality constant C_2 may be found by integrating the probability over all possible orientations and setting it equal to one.

$$\int f(\theta)d\omega = \int_0^{2\pi}\int_0^{\pi} C_2 e^{j_\mathrm{m}H\cos\theta/k_\mathrm{B}T}\sin\theta d\theta d\phi = \frac{4\pi C_2}{\xi}\sinh\xi = 1$$

$$\Rightarrow C_2 = \frac{\xi}{4\pi\sinh\xi} \tag{3.9}$$

In (3.9) term $\xi = j_\mathrm{m}H/k_\mathrm{B}T$ is so called Langevin parameter and it represents the ratio of magnetic and thermal energies. Probability density for a particle magnetic moment to be in an angle θ with the applied field is

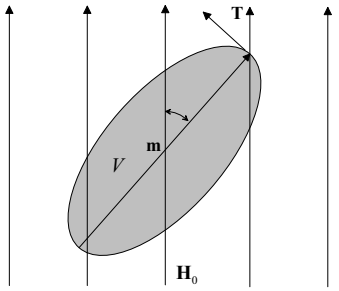

Figure 3.3: Torque $\delta\mathbf{T}$ acting on a single domain magnetic particle in a homogeneous external field $\mathbf{H}_0$. Volume and the magnetic moment of the particle are δV and $\mathbf{m} = \mathbf{j}_\mathrm{m}/\mu_0$, respectively

$$\int f(\theta) = \frac{\xi}{4\pi \sinh \xi} e^{\xi \cos\theta} \tag{3.10}$$

The effective dipole moment of a particle is its component along the field direction, i.e., $\mathbf{j}_\mathrm{m} \cos\theta$. In terms of the probability distribution function $f(\theta)$ the average value of dipole moment is given by

$$\overline{j_\mathrm{m}} =< j_\mathrm{m} \cos\theta >= \frac{\int j_\mathrm{m} \cos\theta f(\theta) d\omega}{\int f(\theta) d\omega} \tag{3.11}$$

Substituting (3.10) in to (3.11) and integrating over all solid angles gives following equation for average dipole moment for particles

$$\overline{j_\mathrm{m}} = j_\mathrm{m} \left[\coth\xi - \frac{1}{\xi} \right] = j_\mathrm{m} \mathcal{L}(\xi) \tag{3.12}$$

Equation (3.12) is called Langevin equation where $\mathcal{L}(\xi)$ is Langevin function.

The magnetization $\mathbf{M}$ of a ferrofluid has the direction of the applied field, and its magnitude is the total of the moments of the magnetic particles suspended in a unit volume of the mixture

$$M = n\frac{\overline{j_\mathrm{m}}}{\mu_0} = n\overline{m} \ , \tag{3.13}$$

where $\overline{m}$ is the component of the mean magnetic moment per particle along the field direction, and n is magnetic particle number density. Similarly, the saturation magnetization M_s of the fluid is given in terms of particle magnetic

moment magnitude m or in terms of saturation moment of bulk magnetic solid M_d and the volume fraction of magnetic solids ϕ by

$$M_s = \phi M_d = nm \tag{3.14}$$

The magnetization **M** of the ferrofluid is a function of the temperature and the magnetic field. The modified variant of the effective field theory (MEFT) (Pshenichnikov and Mekhonoshin, 2000) may be used to describe the equilibrium magnetization of the magnetic fluid. It has proven to be more accurate for higher solid volume fractions than traditional one-particle model where interactions between the particles are neglected. The initial susceptibility χ, defined as M/H, is according to the MEFT

$$\chi = \chi_L(1 + \chi_L/3) \tag{3.15}$$

where $\chi_L = \mu_0 m^2 n/3k_\mathrm{B}T$ is the susceptibility of the one-particle approximation, m is the magnetic moment of a single particle, n is the particle number density, k_B is the Boltzmann constant and T is the absolute temperature. Magnetic fluid susceptibility calculated from Langevin theory, mean effective field theory, and approximate method suggested by Vislovich (Berkovsky et al., 1993)(See also Fig. 1 in Publication VI) is plotted against applied field strength in Figure 3.4. Deviation between the susceptibility predicted by different theories is largest at weak field strengths and diminishes, as expected, when the field strength increases and the magnetization approaches its saturation value.

Temperature dependence of magnetization magnitude M can be divided into three different contributions, namely thermal expansion of carrier fluid, temperature dependence of domain magnetization and disorientation of particles due to temperature difference (Rosensweig et al., 1999).

$$M(T) = \phi(T) M_\mathrm{d}(T) \mathcal{L}(T) \tag{3.16}$$

By the definition, the temperature dependence of magnetic fluid or relative pyromagnetic coefficient β_m, is

$$\beta_\mathrm{m} \equiv -\frac{1}{M}\left(\frac{\partial M}{\partial T}\right). \tag{3.17}$$

Far from the Curie temperature and for strong fields the pyromagnetic coefficient of magnetic fluid is mainly determined by the thermal expansion of the carrier liquid β_c.

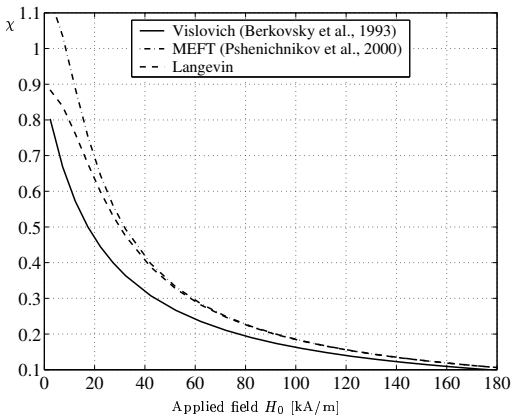

Figure 3.4: Susceptibility of a magnetic fluid calculated using Langevin theory, modified effective field theory and method suggested by Vislovich (Berkovsky et al., 1993).

3.2.1 Magnetic relaxation in ferrofluids

There are two mechanisms by which the magnetization of magnetic fluid may relax after the changes in the applied field. In the first mechanism the relaxation occurs by particle rotation in the liquid. In the second one the relaxation is due to the rotation of magnetic vector within the particle. (Rosensweig, 1997)

The particle rotation is characterized by a Brownian rotational diffusion time τ_{B} having hydrodynamic origin

$$\tau_{\mathrm{B}} = \frac{3V\eta_{\mathrm{f}}}{k_{\mathrm{B}}T}, \tag{3.18}$$

where η_{f} is fluid viscosity, V particle volume and $k_{\mathrm{B}}T$ thermal energy. For a single-domain uniaxial ferromagnetic particle in the absence of magnetic field, the magnetization has two possible orientations, the opposite directions along the easy axis of magnetization. According to Néel an energy barrier must be overcome in order to move from one orientation to the other. Characteristic time for superparamagnetic Néel relaxation τ_{N} is given as

$$\tau_{\mathrm{N}} = \tau_0 \exp\left(\frac{KV}{k_{\mathrm{B}}T}\right), \tag{3.19}$$

where $\tau_0 \sim 10^{-10}$ s and particle anisotropy energy $E_{\mathrm{a}} = KV$ (Raikher et al., 2005). K is an anisotropy constant, measure for the energy of magnet

stored via the interaction of the electron spins with the atomic orbitals in the solid and interactions between adjacent magnets and from the shape of the magnets. Anisotropy constant K for the magnetite Fe_3O_4 is about 40 000 J/m^3. When the condition $E_a \ll k_B T$ is fulfilled, the thermal energy is large enough to induce fluctuations of the magnetization inside the particle with a characteristic time τ_N.

Regardless of experiments (Lederman et al., 1994), which suggests that at room temperature, and in applied fields close to coercivity, the statistics of reversal cannot be described by activation over a single energy barrier as originally proposed by Néel, the Néel's relaxation time can and is frequently used as a reference, when the relaxation of magnetization in magnetic fluids is considered.

When $\tau_N \ll \tau_B$ the relaxation occurs mainly by the Néel mechanism, and the material is said to possess intrinsic superparamagnetism (soft dipole approximation). When $\tau_B \ll \tau_N$, the Brownian mechanism is dominating and the material exhibit extrinsic superparamagnetism (rigid dipole limit).

Comparing relaxation times by rotary diffusion and by internal mechanism the particle diameter for condition $\tau_B = \tau_N$ is found to be in range 5 nm $< d_p <$ 10 nm for typical properties of magnetic fluids. The average particle sizes in commercial magnetic fluids vary from 5 to 12 nm, which means that in a magnetic fluid relaxation may occur by either of the mechanisms or by their combination (Raikher et al., 2005).

4 Numerical methods

4.1 Calculation of magnetic field

Electrical conductivity of magnetic fluids is usually very small and often the fluids can be considered nonconductive. Maxwell equations for a nonconductive material may be written.

$$\nabla \cdot \mathbf{B} = 0 \tag{4.1}$$

$$\nabla \times \mathbf{H} = 0 \tag{4.2}$$

From Equation (4.1) we have an alternative formulation for magnetic field in terms of magnetic scalar potential ϕ_{m}. (Sykulski and Stoll, 1995)

$$\mathbf{H} = -\nabla\phi_{\mathrm{m}} \tag{4.3}$$

By the definition the magnetic induction

$$\mathbf{B} = \mu_0(\mathbf{H} + \mathbf{M}). \tag{4.4}$$

Magnetization of a magnetic fluid is a function of temperature, magnetic field intensity and the concentration of magnetic particles. The magnetic equation of state is linearized about the applied magnetic field, the average temperature and the solid volume fraction of magnetic particles to obtain (Finlayson, 1970)

$$M = M_0 + \frac{\partial M}{\partial H}(H - H_0) + \frac{\partial M}{\partial T}(T - T_0) + \frac{\partial M}{\partial \phi}(\phi - \phi_0) \tag{4.5}$$

Using Maxwell equations with equations (4.3), (4.4) and (4.5) the flux function for magnetic scalar potential may be written as

$$\nabla \cdot \left[\left(1 + \frac{\partial M}{\partial H} \right) \nabla\phi_{\mathrm{m}} \right] = \nabla \cdot \left[\frac{\partial M}{\partial T} \left(T - T_0 \right) + \frac{\partial M}{\partial \phi} \left(\phi - \phi_0 \right) \right]. \tag{4.6}$$

Within the simulation domain $\partial M/\partial H = \chi$, $\partial M/\partial T = -\beta_{\mathrm{m}} M_0$ and $\partial M/\partial \phi$ are assumed constant, in addition differential magnetic permeability is defined $\mu = 1 + \chi$ and (4.6) may be rewritten

$$\nabla \cdot (\mu \nabla \phi_{\mathrm{m}}) = -\beta_{\mathrm{m}} M_0 \nabla \left(T - T_0 \right) + \frac{\partial M}{\partial \phi} \nabla \left(\phi - \phi_0 \right). \tag{4.7}$$

Magnetization of magnetic fluid may be written

$$M = \phi M_{\mathrm{d}} \mathcal{L}(\xi) \ , \tag{4.8}$$

where ϕ is the solid volume fraction of magnetic particles, M_{d} domain magnetization of magnetic material and $\mathcal{L}(\xi)$ is the Langevin function defined as $\mathcal{L}(\xi) = \coth(\xi) - 1/\xi$ and $\xi = \mu_0 m H/(k_B T)$ is the Langevin parameter. From (4.8) we can define the values for χ, β_{m} and $\partial M/\partial\phi$.

$$\left(\frac{\partial M}{\partial H}\right)_{T_0,\phi_0} = \phi_0 M_{\mathrm{d}} \frac{\xi}{H}\left[1 - \coth^2(\xi) + \frac{1}{\xi}\right]. \tag{4.9}$$

$$\left(\frac{\partial M}{\partial T}\right)_{H_0,\phi_0} = -\phi_0 M_{\mathrm{d}} \frac{\xi}{T}\left[1 - \coth^2(\xi) - \frac{1}{\xi^2}\right]. \tag{4.10}$$

$$\left(\frac{\partial M}{\partial \phi}\right)_{H_0,T_0} = M_{\mathrm{d}}\left[\coth(\xi) - \frac{1}{\xi}\right]. \tag{4.11}$$

4.2 Simulations using a single phase approximation

The equations governing the magnetic fluid motions are continuity and momentum equations with thermal energy balance. For small temperature and magnetic field differences the thermodynamic and transport properties of magnetic fluid can be considered constant, except for the density in the gravitational term and the magnetization in the magnetic force term, which are allowed to vary with temperature and latter also with magnetic field magnitude to generate the buoyancy and magnetic force. If the fluid is further assumed incompressible the conservation equations for mass, momentum and energy, for magnetic fluid may be written as

$$\nabla \cdot \mathbf{u} = 0 \tag{4.12}$$

$$\begin{aligned} \rho_0\left(\frac{\partial \mathbf{u}}{\partial t} + \mathbf{u}\cdot\nabla\mathbf{u}\right) &= -\nabla p + \rho(T)\mathbf{g} \\ +\eta\nabla^2\mathbf{u} + \mu_0(\mathbf{M}\cdot\nabla)\mathbf{H} &+ \frac{\mu_0}{2}\nabla\times(\mathbf{M}\times\mathbf{H}) \end{aligned} \tag{4.13}$$

$$\begin{aligned} \left[\rho c_{V,H} - \mu_0\mathbf{H}\cdot\left(\frac{\partial\mathbf{M}}{\partial T}\right)_{V,H}\right]\left(\frac{\partial T}{\partial t} + \mathbf{u}\cdot\nabla T\right) \\ +\mu_0 T\left(\frac{\partial\mathbf{M}}{\partial T}\right)_{V,H}\cdot\frac{\partial\mathbf{H}}{\partial t} = \lambda\nabla^2 T + \mu\Phi \end{aligned} \tag{4.14}$$

Last term in the momentum equation (4.13) represents dissipative or off-equilibrium magnetic force (Müller and Liu, 2001), which is often neglected, when stationary applied fields and small velocities, such as in free convection flows, are considered. Different expressions suggested for the magnetodissipation are presented and discussed in more detail in Chapter 5.3, Equations (5.22) and (5.23). Except for the case presented in Chapter 5.3 and Publication VI (Tynjälä et al., 2002) dissipative term in the momentum equation is neglected throughout this study. For stationary field also the last term on the left hand side of energy equation (4.14) vanishes and due to small velocities the viscous dissipation $\mu\Phi$ may also be neglected (Finlayson, 1970). If we apply the Boussinesq approximation $\rho(T) = \rho_0[1 - \beta(T - T_0)]$ for the density variation in the buoyancy term and use the linearized equation of state $M(T, H) = \chi H_0 - \beta_\mathrm{m} M_0(T - T_0)$ for the magnetization, the governing equations may be written

$$\nabla \cdot \mathbf{u} = 0 \tag{4.15}$$

$$\rho_0 \left(\frac{\partial \mathbf{u}}{\partial t} + \mathbf{u} \cdot \nabla \mathbf{u} \right) = -\nabla p + \rho_0 \beta (T - T_0)\mathbf{g} + \eta \nabla^2 \mathbf{u} + \mu_0 \beta_\mathrm{m} M_0 (T - T_0) \nabla H \tag{4.16}$$

$$\left(\frac{\partial T}{\partial t} + \mathbf{u} \cdot \nabla T \right) = \frac{\lambda}{\rho c_{V,H}} \nabla^2 T \tag{4.17}$$

4.3 Simulations using a mixture model

The mixture model uses a single fluid approach, and can be considered as an intermediate between the single phase approximation and full set of equations governing the dynamics of multiphase flow. In the model the conservation equations for mass, momentum and energy are solved for the mixture. In addition, the mixture model allows the phases to be interpenetrating and to move at different velocities, using the concept of slip velocities. Also the equation of mass conservation for the secondary phase, as well as algebraic expressions for the relative velocities are solved. (Fluent, 2005) To utilize this model the conservation equations are first written for all components of the mixture (Manninen et al., 1996). The continuity, momentum and energy equations for the each phase of the mixture may be written

$$\frac{\partial}{\partial t} (\alpha_i \rho_i) + \nabla \cdot (\alpha_i \rho_i \mathbf{u}_i) = 0. \tag{4.18}$$

$$\frac{\partial}{\partial t}\left(\alpha_i \rho_i \mathbf{u}_i\right) + \nabla \cdot \left(\alpha_i \rho_i \mathbf{u}_i \mathbf{u}_i\right) = -\alpha_i \nabla p_i + \nabla \cdot \left[\alpha_i \left(\tau_i + \tau_{\mathrm{T}i}\right)\right] + \alpha_i \rho_i \mathbf{g} + \alpha_i \frac{\mu_0 m_i}{V_i} \mathcal{L}(\xi) \nabla H + \mathbf{M}_i. \tag{4.19}$$

$$\frac{\partial}{\partial t}\left(\alpha_i \rho_i E_i\right) + \nabla \cdot \left[\alpha_i \mathbf{u}_i \left(\rho_i E_i + p_i\right)\right] = \nabla \cdot \left(\lambda_i \nabla T\right) + S_i. \tag{4.20}$$

Equations for the mixture may be achieved by summation over all of the components. In the case of magnetic fluid there are only two components namely the magnetic phase and the carrier phase with volume fractions equal to α_{p} and α_{c}, respectively. Thus the continuity equation for the mixture may be written

$$\frac{\partial \rho_{\mathrm{m}}}{\partial t} + \nabla \cdot \left(\rho_{\mathrm{m}} \mathbf{u}_{\mathrm{m}}\right) = 0, \tag{4.21}$$

where the mixture density ρ_{m} and velocity $\mathbf{u}_{\mathrm{m}}$ are defined as

$$\rho_{\mathrm{m}} = \sum \left(\alpha_i \rho_i\right) \qquad \mathbf{u}_{\mathrm{m}} = \frac{1}{\rho_{\mathrm{m}}} \sum \left(\alpha_i \rho_i \mathbf{u}_i\right). \tag{4.22}$$

Similarly the momentum (4.23) and energy (4.20) equations for the mixture

$$\frac{\partial}{\partial t}\left(\rho_{\mathrm{m}} \mathbf{u}_{\mathrm{m}}\right) + \nabla \cdot \left(\rho_{\mathrm{m}} \mathbf{u}_{\mathrm{m}} \mathbf{u}_{\mathrm{m}}\right) = -\nabla p_{\mathrm{m}} + \eta \nabla^2 \mathbf{u}_{\mathrm{m}} - \nabla \cdot \left(\alpha_{\mathrm{p}} \rho_{\mathrm{p}} \mathbf{u}_{\mathrm{Mp}} \mathbf{u}_{\mathrm{Mp}} + \alpha_{\mathrm{c}} \rho_{\mathrm{c}} \mathbf{u}_{\mathrm{Mc}} \mathbf{u}_{\mathrm{Mc}}\right) + \rho_{\mathrm{m}} \mathbf{g} + \alpha_{\mathrm{p}} \frac{\mu_0 m_{\mathrm{p}}}{V_{\mathrm{p}}} \mathcal{L}(\xi) \nabla H \tag{4.23}$$

$$\frac{\partial}{\partial t}\left(\rho_{\mathrm{m}} c_{v,\mathrm{m}} T\right) + \nabla \cdot \left[\left(\alpha_{\mathrm{p}} \rho_{\mathrm{p}} \mathbf{u}_{\mathrm{p}} c_{p,\mathrm{p}} + \alpha_{\mathrm{c}} \rho_{\mathrm{c}} \mathbf{u}_{\mathrm{c}} c_{p,\mathrm{c}}\right) T\right] = \nabla \cdot \left(\lambda_{\mathrm{m}} \nabla T\right). \tag{4.24}$$

In Equations (4.23) and (4.20) the subscripts m, p and c refer to the mixture, magnetic particles and the carrier fluid, respectively and $\mathbf{u}_{\mathrm{M}i} = \mathbf{u}_i - \mathbf{u}_{\mathrm{m}}$ is the diffusion velocity.

The mass conservation equation for magnetic particles may be written

$$\frac{\partial}{\partial t}\left(\alpha_{\mathrm{p}} \rho_{\mathrm{p}}\right) + \nabla \cdot \left(\alpha_{\mathrm{p}} \rho_{\mathrm{p}} \mathbf{u}_{\mathrm{m}} - \mathbf{j}_{\mathrm{p}}\right) = 0, \tag{4.25}$$

where $\mathbf{j}_p$ is the flux of magnetic grains. In the presence of temperature or concentration gradient the mass transfer of magnetic particles in magnetic

fluid may occur due to thermal and Brownian diffusion. In the presence of both temperature and concentration gradient the flux of magnetic particles may be written

$$\mathbf{j}_\mathrm{p} = \alpha_\mathrm{p} \left(\mathbf{u}_\mathrm{p} - \mathbf{u}_\mathrm{c}\right) - D \left(\nabla \alpha_\mathrm{p} + S_\mathrm{T} \nabla T\right), \tag{4.26}$$

where D is the Brownian diffusion coefficient defined as $D = k_\mathrm{B}T/6\pi\eta d_\mathrm{p}$, D_T is the thermal diffusion coefficient and $S_\mathrm{T} = D_\mathrm{T}/D$ is so called Sóret coefficient taking account for the particle flux caused by the temperature difference within the fluid (Blums and Odenbach, 2000).

According to the Newton's second law the acceleration of mass is equal to the sum of forces acting on mass. If we consider forces acting on a single magnetic particle, we can define the slip velocity $\mathbf{u}_\mathrm{s} = \mathbf{u}_\mathrm{p} - \mathbf{u}_\mathrm{c}$ between the phases

$$\rho_\mathrm{p} V_\mathrm{p} \frac{\partial \mathbf{u}_\mathrm{s}}{\partial t} = \mu_0 m_\mathrm{p} \mathcal{L}(\xi) \nabla H + V_\mathrm{p} \left(\rho_\mathrm{p} - \rho_\mathrm{c}\right) \mathbf{g} - 6\pi\eta r_\mathrm{p} \mathbf{u}_\mathrm{s}, \tag{4.27}$$

where the Stokes drag coefficient, presented in Chapter 2.1.1, valid for low particle Reynolds numbers is applied. At equilibrium the terminal slip velocity for spherical particles may be written as

$$\mathbf{u}_\mathrm{s} = \frac{\mu_0 m_\mathrm{p} \mathcal{L}(\xi)}{3\pi\eta d_\mathrm{p}} \nabla H + \frac{d_\mathrm{p}^2 \left(\rho_\mathrm{p} - \rho_\mathrm{c}\right)}{18\pi\eta} \mathbf{g}. \tag{4.28}$$

Use of Equation (4.28) requires that local equilibrium condition is fulfilled. The local equilibrium approximation assumes that particles are accelerated rapidly to the terminal velocity (Manninen et al., 1996).

4.4 Discretization methods

To find a numerical solution to differential equations presented in previous sections, the continuum problem with infinite number of degrees of freedom should be reduced to a discrete problem with finite number of degrees of freedom and described by system of algebraic equations. (Fidap, 1998) In most methods, the calculation domain of interest, is divided into small simply shaped regions called elements or cells.

Numerical simulations presented in Chapter 5 and in the attached Publications V and VI, have been produced using commercial Fidap software, and Publications I to IV using commercial Fluent software[1]. Fidap uses finite element simulation method (FEM) and Fluent uses so called finite volume

[1]Both softwares are registered trademarks of Fluent Inc. More information http://www.fluent.com

(FVM) or control volume method. The methods and procedures used in this work are briefly described in the following sections.

4.4.1 Finite element method

In finite element method the calculation domain is divided into elements. Values for dependent variables $u, v, w, T, p, \phi, \phi_{\mathrm{m}}$ are defined in discrete node points of elements and within each element the values are interpolated by functions typically first or second order. Within each element, e.g. velocity, pressure and temperature fields are approximated by (Fidap, 1998)

$$\begin{aligned} u_i(x,t) &= \varphi^{\mathrm{T}}\mathbf{U}_i(t) \\ p(x,t) &= \psi^{\mathrm{T}}\mathbf{P}(t) \\ T(x,t) &= \vartheta^{\mathrm{T}}\mathbf{T}(t), \end{aligned} \tag{4.29}$$

where $\mathbf{U}_i, \mathbf{P}$ and $\mathbf{T}$ are column vectors of element nodal point unknowns and φ, ψ, and ϑ are column vectors of the interpolation functions. Substitution of approximations shown in equation (4.30), into differential equations for momentum, mass and energy conservation yields a set of equations

$$\begin{aligned} \mathbf{R}_1 &= \mathbf{f}_1(\varphi, \psi, \vartheta, \mathbf{U}_i, \mathbf{P}, \mathbf{T}) \\ \mathbf{R}_2 &= \mathbf{f}_2(\varphi, \psi, \vartheta, \mathbf{U}_i, \mathbf{P}, \mathbf{T}) \\ \mathbf{R}_3 &= \mathbf{f}_3(\varphi, \psi, \vartheta, \mathbf{U}_i, \mathbf{P}, \mathbf{T}), \end{aligned} \tag{4.30}$$

where residual vector $\mathbf{R}$ results from the errors caused by approximations made in interpolation, Equation (4.30). Objective in numerical simulation is to minimize this residual vector. Method of weighted residuals (Patankar, 1980) solves equation

$$\int_V \mathbf{R} \cdot \mathbf{W} dV = 0, \tag{4.31}$$

where $\mathbf{W}$ is the weighting function vector and the integration is performed over the domain of interest. Finite element method uses the Galerkin form of the method of weighted residuals (Finlayson, 1970), where the objective is to make residuals orthogonal to the interpolation functions of each element (Fidap, 1998). In other words, as an weighting functions of equation (4.31), the interpolation functions φ, ψ, and ϑ are used. Orthogonality conditions for momentum, mass and energy conservation may be expressed by

$$\begin{aligned} \int_V \mathbf{R}_1 \cdot \varphi &= 0 \\ \int_V \mathbf{R}_2 \cdot \psi &= 0 \\ \int_V \mathbf{R}_3 \cdot \vartheta &= 0. \end{aligned} \tag{4.32}$$

The application of the Galerkin finite element procedure produces a set of nonlinear algebraic equations. The group of equations is traditionally solved simultaneously, using fully coupled approach. The coupled method is cost effective for majority of two-dimensional problems, but requires lots of memory to store the system matrix. Fully coupled algorithm is too heavy for practically all three-dimensional problems and for problems with large number of degrees of freedoms.

Instead of coupled, an iterative segregated solution method was used in the simulations. In segregated solver the governing non-linear and coupled equations are solved separately in a sequential manner (Fidap, 1998). The segregated approach substantially reduces disk storage requirements compared to fully coupled algorithm. The cost of memory saving is paid by increased number of iterations required to obtain converged solution in segregated solvers compared to coupled algorithms. (Fidap, 1998)

In both cases studied with FEM (Publications V and VI), the magnetic fluid was assumed homogenous and isotropic using single phase equations, presented in Section 4.2. In addition, a method called penalty formulation, was employed. In penalty approach small imbalance, determined by penalty parameter ϵ, is allowed to continuity equation. Parameter ϵ is very small, typically order of 10^{-9} to 10^{-5} and the continuity equation (4.15), is replaced by the equation

$$\nabla \cdot \mathbf{u} = \epsilon p. \tag{4.33}$$

Equation (4.33) is used to eliminate the pressure p from the momentum equation. (Fidap, 1998)

4.4.2 Finite volume method

Finite volume method is actually a special case of method of weighted residuals. In finite volume method the weighting function W is set equal to unity over one subdomain at a time and zero everywhere else. In finite volume or control volume method the integral of the residual over each control volume must become zero (Patankar, 1980).

In the finite volume simulations so called Semi-Implicit Method for Pressure Linked Equations (SIMPLE) (Patankar and Spalding, 1972; Patankar, 1980), was used.

SIMPLE is segregated method. Actual velocities u, v, w and pressure p have been divided into simulated or guessed value u^*, v^*, w^*, p^* and correction term u', v', w', p'

$$\begin{aligned} p &= p^* + p' \\ u &= u^* + u' \\ v &= v^* + v' \\ w &= w^* + w' \end{aligned} \tag{4.34}$$

In the method, the momentum conservation equations are first solved for velocities, based on earlier simulations or initial guesses of velocity and pressure fields. Obtained velocity field doesn't necessarily satisfy the continuity equation. Pressure correction term p' is calculated from the continuity equation and corresponding new pressure field is obtained $p = p^* + p'$. Velocity field is corrected with velocity correction term calculated with new pressure field and velocity fields $[u, v, w] = [u^*, v^*, w^*] + [u', v', w']$ are obtained. Detailed description of the method, and equations for the pressure and the velocity correction can be found from (Patankar, 1980) and (Patankar and Spalding, 1972).

Then discretization equations for other dependent variables (such as T, ϕ, ϕ_m) are calculated as well as disperse phase continuity equation and algebraic equations e.g. for slip velocity and temperature, field and/or concentration dependent fluid properties are updated before new iteration round is started. Several iterations of the solution loop are required before converged solution is obtained for a steady state problem or for a single time step of an unsteady problem. Solution procedure is illustrated in Figure 4.1.

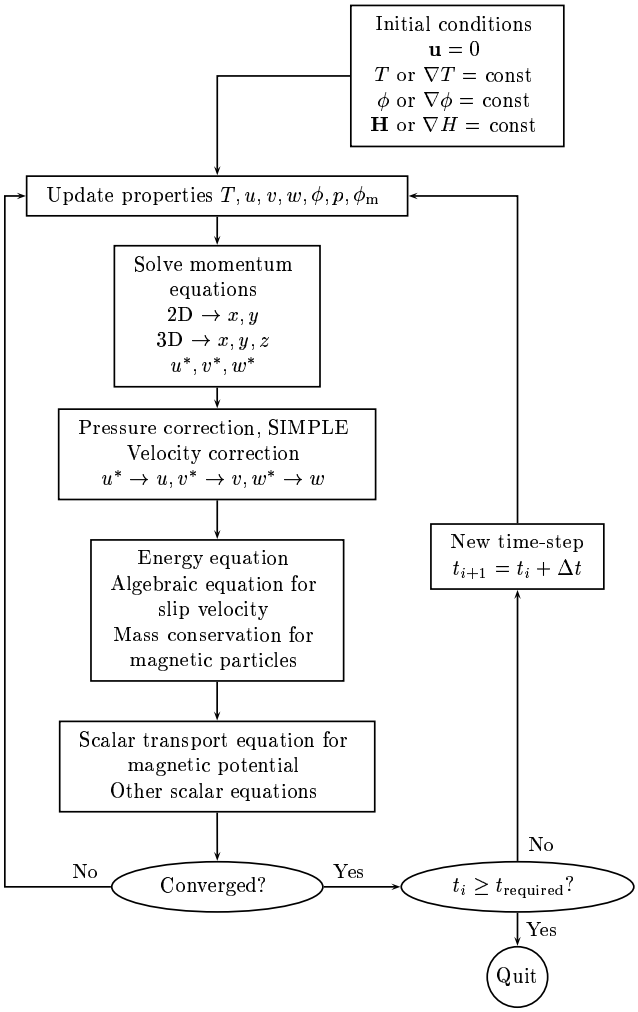

Figure 4.1: Solution procedure of segregated solution method used in the finite volume simulations.

5 Studied cases

In this section the studied cases and methods used in the studies have been presented. In order to evaluate different theories and simulation models, magnetic fluid convection was studied in shallow circular cylinder, in cylindrical annulus and in triangular cavity. First mentioned case was studied using two-phase mixture model Chapter 5.1 and cases of cylindrical annulus and triangular enclosure cases Chapters 5.2 and 5.3 were studied using standard single phase approach for stable magnetic fluids. Related publications can be found from appendices I to VI. Table 5.1 summarizes studied cases and methods used in different papers.

Appendices VII and VIII are related to particle dynamics simulations of granular flows using modified hard-sphere algorithm. Results of these publications have been published and extensively reported in two earlier Doctoral Thesis by Jalali (2000) and Zamankhan (2004), and are not discussed here. Some features, typical for complex systems and common for both colloidal suspensions and macroscopic systems, like granular flows, as well as methods of analysis used in studies, have been presented in Chapter 2.

Simulations were mainly conducted using SGI Origin 2000 computer[2] at premises of CSC - Scientific Computing LTD [3]. The computer has 128 processors of clock frequency 300 MHz. Theoretical peak performance is 76.8 Gflop/s and total amount of memory 160 GB. Some smaller cases were simulated using desktop PC's.

As outlined in previous chapter, the simulation algorithms were based on commercial finite element (FIDAP) and finite volume (Fluent) softwares, and user defined functions were applied to take account for the special properties of magnetic fluids.

Table 5.1: Investigated cases, methods and models used in the studies.

Chapter/ Appendix	**Geometry**	**Method**	**Single phase Two-phase**	**Steady Unsteady**	**Other**
5.1/I	Disk	FVM	SP/TP	US	$\mathbf{H} = 0$
5.1/II	Disk	FVM	SP/TP	US	–
5.1/III	Disk	FVM	SP/TP	US	–
5.1/IV	Disk	FVM	SP/TP	US	$\mathbf{H} = 0$
5.2/V	Annular	FEM,FVM	SP	ST/US	–
5.3/VI	Triangular	FEM	SP	ST	Diss.

[2]Manufacturer Silicon Graphics Inc. http://www.sgi.com
[3]Center for Scientific Computing in Finland. http://www.csc.fi

5.1 Shallow circular cylinder

Rayleigh convection in a shallow circular disk was studied by numerical simulations and simulation results were validated against experimental results. The case was studied both in the absence of magnetic field, Publications I and IV, (Tynjälä et al., 2005; Bozhko et al., 2005), and with applied uniform transversal magnetic field, Publications II and III, (Bozhko and Tynjälä, 2005; Bozhko et al., 2004). Schematic of the studied case is shown in Figure 5.1.

The stability of mechanical equilibrium as well as intensity of convective motion of non-isothermal magnetic fluid subjected to gravity and magnetic fields are determined by gravitational and magnetic Rayleigh numbers, Ra_{g} and Ra_{m}, defined as,

$$Ra_{\mathrm{g}} = \frac{g\beta\Delta T h^3}{\nu\kappa} \tag{5.1}$$

$$Ra_{\mathrm{m}} = \frac{\mu_0(\beta_{\mathrm{m}} M \Delta T h)^2}{\rho\nu\kappa(1+\chi)}, \tag{5.2}$$

where ΔT is the temperature difference across the fluid layer, h is the layer thickness and g is the acceleration due to the gravity. β and β_{m} are thermal expansion and relative pyromagnetic coefficient, respectively. M, χ and ρ are the magnetization, susceptibility, and density of magnetic fluid and μ_0 is the vacuum permeability. From the relationship of control parameters $Ra_{\mathrm{m}}/Ra_{\mathrm{g}} \sim M^2\Delta T/h$ it is visible that in order to promote the role of magnetic mechanism on experiments on earth gravity field, it is better to use thin layers, large temperature differences and medium with high values of magnetization (Bozhko et al., 2004).

In comparison to the pure fluid case, the dynamics and bifurcation scenario in binary mixtures are more complicated due to the extra degree of freedom associated with the concentration field Ryskin et al. (2003). The concentration gradients of magnetic particles may be developed due to the gravitational settling of magnetic particles and their aggregates or, when temperature or magnetic field gradients are present, due to thermal diffusion (Soret effect) and magnetophoresis (Blums, 1995), respectively.

In the absence of magnetic field and in the presence of temperature gradient the flux of magnetic particles is influenced by the gravitational sedimentation as well as Brownian and thermal diffusions. Due to thermal diffusion the particles may migrate towards lower or higher temperature, corresponding to positive or negative Soret coefficients. For surfacted ferrofluids used in this study the Soret coefficients have been found positive (Blums et al., 1997;

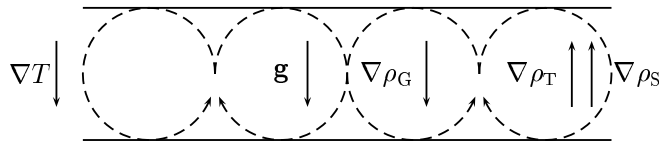

Figure 5.1: Temperature gradient ∇T applied to layer of binary fluid with positive separation ratio ψ. Density gradients due to Soret effect $\nabla \rho_S$ and carrier fluid expansion $\nabla \rho_T$ are coaligned leading to potentially unstable heavy fluid top system.

Lenglet et al., 2002).

The case has been recently studied theoretically by Ryskin et al. both in the absence (Ryskin et al., 2003) and in the presence of magnetic field (Ryskin and Pleiner, 2004). In the absence of field the analysis Ryskin et al. (2003) suggested that the convection instability for the positive Soret coefficient remains stationary and an oscillatory instability occurs only in binary fluids with negative Soret coefficient. In contrary, recent theoretical analysis of Huke and Lücke (2005) revealed the presence of rolls, squares, cross-rolls, as well as oscillatory cross-rolls, in the Rayleigh convection of magnetic fluid with positive S_T and very small Lewis number $Le = D/\kappa$.

5.1.1 Governing equations

Numerical simulations were conducted using a finite volume simulation method, where the governing equations are integrated about each control volume, resulting discrete equations that conserve each quantity on a control-volume basis. Second-order upwind scheme was used for continuity, momentum and energy equations, whereas the first order scheme was used for the calculation of magnetic potential and the SIMPLE algorithm described in Chapter 4, was used for the pressure-velocity coupling. Second order implicit method was used for time discretization in simulated unsteady cases.

In the simulations a two-phase mixture model was used Bozhko et al. (2004). In the model the ferrofluid is treated as a two-phase mixture of magnetic particles in a carrier phase. In the model the conservation equations for mass, momentum and energy are solved for the mixture phase. In addition, a mass conservation equation for the suspended particles and an algebraic expression for the relative velocity between the fluid and particles are solved (Manninen et al., 1996). As described in Section 4.3, the continuity, momentum and energy equations for the mixture may be written,

$$\frac{\partial \rho_{\mathrm{m}}}{\partial t} + \nabla \cdot (\rho_{\mathrm{m}} \mathbf{u}_{\mathrm{m}}) = 0 \ , \tag{5.3}$$

$$\frac{\partial}{\partial t} (\rho_{\mathrm{m}} \mathbf{u}_{\mathrm{m}}) + \nabla \cdot (\rho_{\mathrm{m}} \mathbf{u}_{\mathrm{m}} \mathbf{u}_{\mathrm{m}}) = -\nabla p_{\mathrm{m}} + \eta \nabla^2 \mathbf{u}_{\mathrm{m}}$$

$$-\nabla \cdot (\alpha_{\mathrm{p}} \rho_{\mathrm{p}} \mathbf{u}_{\mathrm{Mp}} \mathbf{u}_{\mathrm{Mp}} + \alpha_{\mathrm{c}} \rho_{\mathrm{c}} \mathbf{u}_{\mathrm{Mc}} \mathbf{u}_{\mathrm{Mc}}) + \rho_{\mathrm{m}} \mathbf{g} + \frac{\mu_0 m_{\mathrm{p}}}{V} \mathcal{L}(\xi) \nabla H \ , \tag{5.4}$$

$$\frac{\partial}{\partial t} (\rho_{\mathrm{m}} c_{v,\mathrm{m}} T) + \nabla \cdot \left[(\alpha_{\mathrm{p}} \rho_{\mathrm{p}} \mathbf{u}_{\mathrm{p}} c_{p,\mathrm{p}} + \alpha_{\mathrm{c}} \rho_{\mathrm{c}} \mathbf{u}_{\mathrm{c}} c_{p,\mathrm{c}}) \, T \right] = \nabla \cdot (\lambda_{\mathrm{m}} \nabla T) \, , \tag{5.5}$$

The mass conservation equation for magnetic particles is

$$\frac{\partial}{\partial t} (\alpha_{\mathrm{p}} \rho_{\mathrm{p}}) + \nabla \cdot \left(\alpha_{\mathrm{p}} \rho_{\mathrm{p}} \mathbf{u}_{\mathrm{m}} - \mathbf{j}_{\mathrm{p}} \right) = 0, \tag{5.6}$$

where $\mathbf{j}_p$ is the flux of magnetic grains. In the presence of temperature or concentration gradients the mass transfer of magnetic particles in magnetic fluid may occur due to thermal or Brownian diffusion.

Assuming local equilibrium conditions and Stokesian drag the equation for slip velocity reduces to

$$\mathbf{u}_{\mathrm{s}} = \frac{\mu_0 m_{\mathrm{p}} \mathcal{L}(\xi)}{3\pi\eta d_{\mathrm{p}}} \nabla H + \frac{d_{\mathrm{p}}^2 \, (\rho_{\mathrm{p}} - \rho_{\mathrm{c}})}{18\pi\eta} \mathbf{g}. \tag{5.7}$$

And finally the magnetic field and field gradient inside the simulation domain may be calculated from the scalar transport equation for magnetic potential

$$\nabla \cdot (\mu \nabla \phi_{\mathrm{m}}) = -\beta_{\mathrm{m}} M_0 \nabla \, (T - T_0) + \frac{\partial M}{\partial \phi} \nabla \, (\phi - \phi_0) \, . \tag{5.8}$$

5.1.2 Simulation mesh and mesh quality

The results of thermal convection simulations in a cavity of large aspect ratio are very sensitive to mesh selection and too coarse mesh will lead to convective patterns following the mesh structure. In numerical methods one has to make a compromise between the accuracy of the results and the computational costs.

In the simulations, mesh with total number of 253 119 tetrahedral volumes, was used. Trial cases were run with hexahedral mesh and for various mesh

Table 5.2: The overall relationship between Q_{EAS} and the element quality (Fluent, 2004) and percentage of mesh volumes for each range in the mesh used in the simulations.

Q_{EAS}	Quality	Percent
0	Equilateral (Perfect)	0
$0 < Q_{\mathrm{EAS}} \leq 0.25$	Excellent	16.85
$0.25 < Q_{\mathrm{EAS}} \leq 0.5$	Good	76.91
$0.5 < Q_{\mathrm{EAS}} \leq 0.75$	Fair	6.19
$0.75 < Q_{\mathrm{EAS}} \leq 0.9$	Poor	0.05
$0.9 < Q_{\mathrm{EAS}} < 1$	Very poor	0
1	Degenerate	0

densities. Tetrahedral mesh with triangular face elements provided evenly distributed mesh for the considered cylindrical geometry, in which also the velocity magnitude is distributed evenly without sharp gradients.

Besides trial and error method, the mesh quality was evaluated by calculating EquiAngleSkew Q_{EAS} (Fluent, 2004). Q_{EAS} is a normalized measure of skewness that is defined as follows:

$$Q_{\mathrm{EAS}} = \max\left\{\frac{\theta_{\max} - \theta_{\mathrm{eq}}}{180^\circ - \theta_{\mathrm{eq}}}, \frac{\theta_{\mathrm{eq}} - \theta_{\min}}{\theta_{\mathrm{eq}}}\right\}, \tag{5.9}$$

where $\theta_{\max}$ and $\theta_{\min}$ are the maximum and minimum angles between edges of the element and θ_{eq} is the characteristic angle corresponding to an equilateral cell of similar form. For triangular and tetrahedral elements $\theta_{\mathrm{eq}} = 60^\circ$.

By definition, $0 \leq Q_{\mathrm{EAS}} \leq 1$, and for perfectly equilateral element $Q_{\mathrm{EAS}} = 0$ and completely degenerate $Q_{\mathrm{EAS}} = 1$. Table 5.2 presents the overall relationship between Q_{EAS} and the element quality (Fluent, 2004) and percentage of mesh volumes for each range in the mesh used in the simulations.

5.1.3 Initial and boundary conditions

The simulations were carried out first for initially homogeneous distribution of particles (5.10) and then for initial concentration gradient evaluated from the simulated large particle sedimentation profile shown in Figure 5.2. Figure 5.2 presents numerical results of gravitational sedimentation of 100 nm particles or drop aggregates of particles, for temperature difference less than critical temperature difference for initially homogeneous fluid. In the simulations the initial temperature distribution from the conduction solution is applied, which can be seen from small increase in cooler regions in solid volume fraction shortly after simulation startup. Later the particles start to

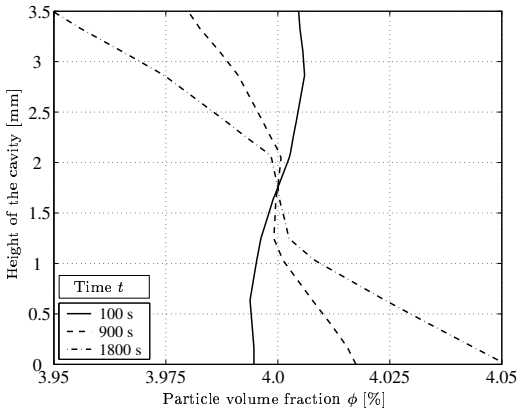

Figure 5.2: Sedimentation of particles as function of time for $\Delta T < \Delta T_{\mathrm{C}}$ for initially homogeneous particle concentration of $\phi = 4\%$.

sedimentate slowly because buoyancy is not large enough to start the convective motion. Particle volume fraction profiles corresponds to 100 s, 900 s and 1800 s. Particle diameter in the simulations was 100 nm in order to imitate spherical aggregates, which may actually contain thousands of particles (Buzmakov and Pshenichnikov, 1996; Pshenichnikov and Mekhonoshin, 2000).

Based on Figure 5.2 an initial sedimentation gradient of $d\phi/dz = -0.3\ 1/\mathrm{m}$ was applied in selected cases to simulate the fluid been at rest for several days. As an initial temperature distribution, either initially constant temperature or the conduction solution of the problem (5.13) was used.

$$\phi = \phi_0, \tag{5.10}$$

$$\phi(z) = \phi_0 - 0.3z, \tag{5.11}$$

$$T = T_{\mathrm{C}}, \tag{5.12}$$

$$T(z) = T_0 - \frac{T_{\mathrm{H}} - T_{\mathrm{C}}}{h} z, \tag{5.13}$$

Constant temperature boundary conditions were applied for both bottom and top surfaces of the cavity, the sidewalls were insulated and no-slip condition for velocity was used for all boundaries.

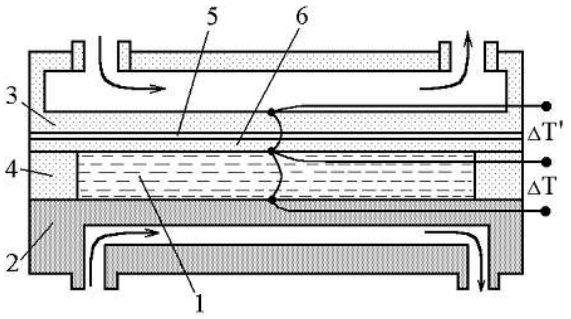

Figure 5.3: Experimental setup, 1 - ferrofluid, 2, 3 – copper and plexiglas exchangers, 4– ring framework, 5 – liquid crystal film, 6– protective plate. (Bozhko and Putin, 2003)

$$u = 0, \ \frac{dT}{dr} = 0, \ \text{at } r = D/2. \tag{5.14}$$

$$u = 0, \ T = T_{\mathrm{C}}, \ \text{at } z = h. \tag{5.15}$$

$$u = 0, \ T = T_{\mathrm{H}}, \ \text{at } z = 0. \tag{5.16}$$

5.1.4 Experimental setup and fluid properties

Experimental setup is presented in Figure 5.3 (Bozhko and Putin, 2003). To observe the convection patterns the cylindrical fluid layer of thickness $h = 3.50 \pm 0.03$ mm and diameter 75 mm was used. The bottom surface of the layer was a copper exchanger with the channels for constant-temperature circulating water. The top transparent heat exchanger was composed of plexiglas parallel plates, which were separated by a gap for pumping of thermostat water. The circular sidewall of the layer was made of Plexiglas. The liquid crystal sheet of 0.1 mm thick was used for the visualization of convection patterns. The liquid crystal undergoes its entire color change from approximately 24 to 27°C from brown to blue color. The temperature oscillations were registered using thermocouples and by visual observations with the help of a video camera. More detailed description of the setup can be found in (Bozhko and Putin, 2003) and references therein.

Experiments were performed for a kerosene-based magnetic fluid containing magnetite Fe_3O_4 particles. Magnetic phase concentration was 10 % and fluid saturation magnetization $M_{\mathrm{s}} = 48$ kA/m, in most of the simulations. Some

comparisons were made with weak concentration magnetic fluid for which, $\rho = 980$ kg/m^3, $M_s = 15$ kA/m and magnetic phase concentration $\phi \approx 4$ %.

Other physical properties of the studied magnetic fluid were approximately as follows: thermal expansion coefficient $\beta = 0.0002$ 1/K, dynamical viscosity in the absence of field $\eta = 6$ kg/ms, heat capacity $c_p = 2000$ J/kgK, heat conductivity $\lambda = 1$ W/mK. In the simulations all physical properties, except density, were considered constant and determined at average temperature, solid volume fraction and magnetic field.

Mean size of the magnetite particles in the studied fluid was 10 nm. In the simulations particle diameter was varied from 10 to 100 nm in order to study the effect of larger particles or formation of clusters. Relatively large value of initial susceptibility $\chi_0 = 5.7$ indeed indicates that the formation of aggregates may occur in the studied fluid. Effective particle size was determined based on the measured initial susceptibility assuming homogeneous and isotropic distribution of spherical particles. Effective particle diameter of 17 nm was found from the Equation (3.15), based on measured initial susceptibility. This finding is in agreement with the experiments of Thurm and Odenbach (2002), which indicated that for commercial magnetic fluids the increase in field-dependent viscosity is higher that one would theoretically expect based on the size distribution of particles in fluid. Explanation for this phenomena has been thought to be related to the magnetically hard large particles and their agglomerates (Thurm and Odenbach, 2002).

5.1.5 Results and discussion

In the experiments oscillatory convection was observed in the entire investigated temperature region. In contrast to the single component fluid, the convection in ferrofluid appears "hard" and with hysteresis. When temperature difference is increased quasistatically, the convection starts at $\Delta T > \Delta T_{cr}$ and ΔT_{cr} changes within wide limits in the dependence of experiment prehistory. The reproducible critical temperature $\Delta T_{cr} = 4.5$ K turns out at decreasing ΔT. Figure 5.4 illustrates the dependence of local Nusselt number as a function of applied temperature difference ΔT. The inclined segments in Figure 5.4 connect minimal and maximal values of oscillatory heat flux during experiments ran at fixed temperatures of the heat exchangers. The narrow hysteresis loop shown by arrows on the insert of Figure 5.4, corresponds to the case of beforehand convection-mixed fluid. For initially "non-mixed" colloid the hysteresis depth can widen to $3 \times \Delta T_{cr}$.

Numerical simulations revealed the onset of either steady or unsteady oscillatory convection determined by the initial concentration gradient and size of the particles in the fluid. Figure 5.5 shows the time dependence of heat flux

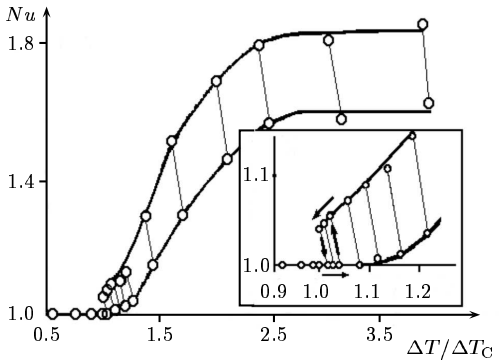

Figure 5.4: Transition from quiescent state to convection and back in a horizontal ferrofluid layer. The insert demonstrates the hysteresis near the onset of convection. (Bozhko and Putin, 2003), Publication I

obtained from numerical simulations. Heat fluxes of different cases have been normalized using the mean value of heat flux of the corresponding case. The simulations were carried out for initially homogeneous distribution of particles and for fluid with initial concentration gradient. When initial concentration gradient was applied, the mixture model simulations revealed chaotic convection patterns as shown by solid line in Figure 5.5. Close to critical Rayleigh numbers, competing actions of buoyancy and gravity lead to large fluctuations in the simulated heat flux signal. Simulations near the onset of convection are very time consuming and the duration of simulations is not long enough to make detailed statistical analysis. However, the maximum magnitude of heat flux fluctuations obtained from the simulations with initial concentration gradient $d\phi/dz = -0.3$ 1/m and temperature difference $\Delta T/\Delta T_{\rm cr} \approx 2$, were about $\pm 5\%$ from the mean value, which corresponds well with the magnitude observed experimentally. Simulations for initially homogeneous fluid (dashed line) and for larger temperature differences (dotted line) in Figure 5.5, lead to steady oscillatory convection.

Figure 5.6 represents case with numerical oscillations in otherwise steady case. Applying a disturbance in stable system shows only short peak in heat flux signal and system stabilizes back to mean value. Oscillations disappear after disturbance, which alludes to numerical nature of small sawtooth oscillations before disturbance. However, similar behavior was observed in the experiments, where for non-mixed fluid been at rest the oscillatory convection appeared and oscillations disappeared first after applying large temperature difference for short period of time to mix the fluid.

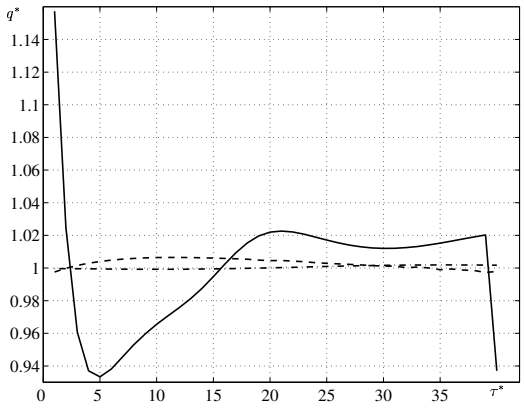

Figure 5.5: Development of the normalized heat flux q^* as a function of dimensionless time τ^*. Solid line represents case with initial concentration gradient $d\phi/dz = -0.3$ 1/m and $\Delta T/\Delta T_{\mathrm{cr}} \approx 2$, dashed line is the case with $d\phi/dz = -0.3$ 1/m and $\Delta T/\Delta T_{\mathrm{cr}} \approx 5$ and dotted line - initially homogeneous concentration of magnetic particles at $\Delta T/\Delta T_{\mathrm{cr}} \approx 5$.

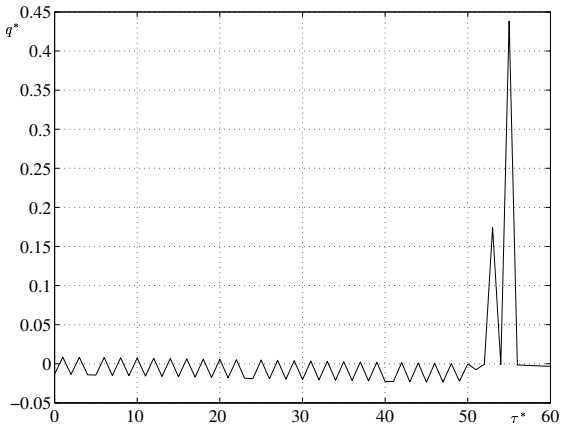

Figure 5.6: Applying a disturbance in stable system shows only short peak in heat flux signal and system stabilizes back to mean value. Oscillations disappear after disturbance, which alludes to numerical nature of small sawtooth oscillations before disturbance

Experimentally observed spatiotemporal convection patterns at $\Delta T = 2.1\times$ $\Delta T_{\rm cr}$ are shown in Figures 5.7 (a) and (b). Figures 5.7 (c) and (d) present simulated convection patterns for corresponding case. Patterns consist of disordered convection rolls and cells which spontaneously appear and disappear. The breaking-up of the roll pairs, such as in Figures 5.7 (a) and (c) and their subsequent partial recombination proceed through a cellular structure, shown in Figures 5.7 (b) and (d). Previously similar behavior were observed for binary mixture and it is known as "zipper state" Bestehorn et al. (1980). The sample of temperature oscillations recorded at this ΔT is shown in Figure 5.8 (a).

In order to study the nature of spatiotemporal variations of the temperature oscillations, wavelet analysis were conducted for the temperature signals. Temperature signals of selected cases and corresponding wavelet-transforms are presented in Figures 5.8 (a), (b) and (c). Wavelet-analysis revealed that along with periods 8 - 15 min there are periods from 1 to 6 hours. The existence of large and small periods is typical for other values of ΔT as well. As to the time evolution of patterns there are slow movement of roll systems as a whole and high-speed reconstruction of the convection rolls because of the cross-roll instability. The behavior of weak concentration magnetic fluid ($\rho = 980$ kg/m^3, $M_{\rm s} = 15$ kA/m and $\Delta T_{\rm cr} = 3,0$ K) presented in Figure 5.8 (c), differs from the strong concentration ones shown in Figures 5.8 (a) and (b). In fluid with small volume fraction of magnetic particles the convection rolls are nearly stationary after initial disturbances disappear. Figure 5.9 demonstrates the establishment of convection rolls in weak concentration magnetic fluid, for $\Delta T = 3.7 \times \Delta T_{\rm cr}$, corresponding to temperature signal shown in Figure 5.8 (c). For half an hour the small defects of the convection structure appear and disappear and after that the flow is nearly stationary for 5 hours.

5.1.6 Effect of magnetic field

All previous results were obtained in the absence of applied magnetic field. In the presence of magnetic field the case is essentially more complex, even if the applied magnetic field is uniform as in this case. Finlayson (1970) was the first to study theoretically the thermomagnetic convection instability in a presence of homogeneous vertical magnetic field. Through the temperature-dependence of magnetic susceptibility the thermal gradient renders an internal magnetic field gradient working as a driving force for the convection.

However, in first experiments (Bogatyrev and Shaidurov, 1976) it was revealed that magnetic field exerts a stabilizing influence on the onset of convection. The experimental investigations (Bozhko and Putin, 1991) have

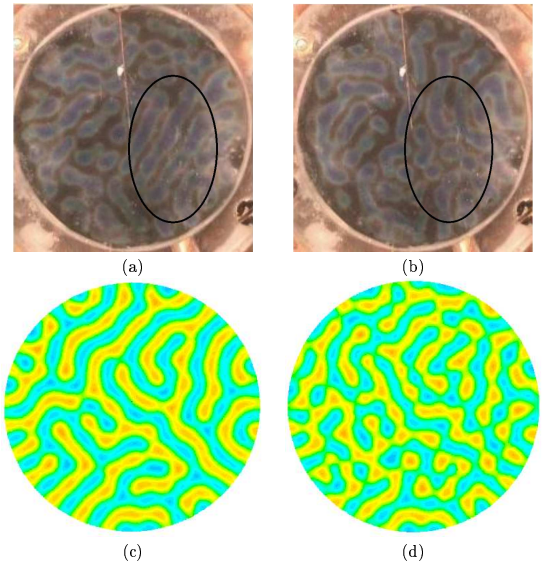

Figure 5.7: Convection patterns in ferrofluid at $\Delta T/\Delta T_{\rm cr} \approx 2$: (a), (b) - liquid crystal visualization; (c), (d) -numerical simulations. The time interval between snapshots: (a), (b) - 30 min; (c), (d) - 15 min. Photos by Dr. A. Bozhko, PSU.

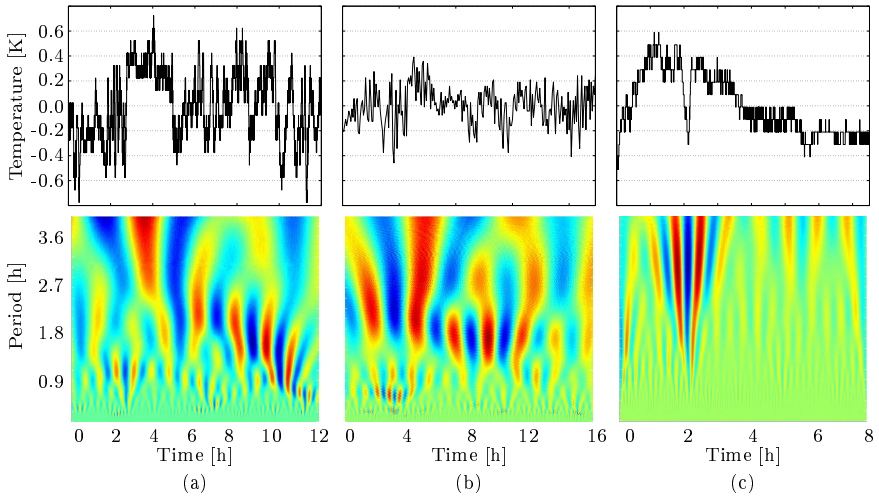

Figure 5.8: Fluctuation components of temperature oscillations and corresponding wavelet transforms for (a) $\phi = 10\%$, $\Delta T = 2.1 \times \Delta T_{\rm cr}$ (b) $\phi = 10\%$, $\Delta T = 1.5 \times \Delta T_{\rm cr}$ and (c) $\phi \simeq 4\%$, $\Delta T = 3.7 \times \Delta T_{\rm cr}$

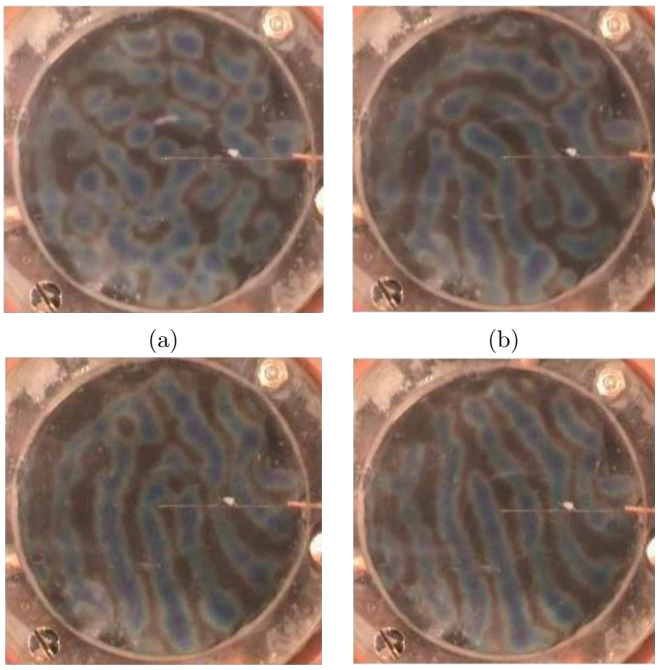

(a) (b)

(c) (d)

Figure 5.9: Transition to stationary flow at $\Delta T = 3.7 \times \Delta T_{\mathrm{cr}}$. The time intervals between the snapshots: a), b) - 25 min, b), c), d) - 1 hour. Photos by Dr. A. Bozhko, PSU.

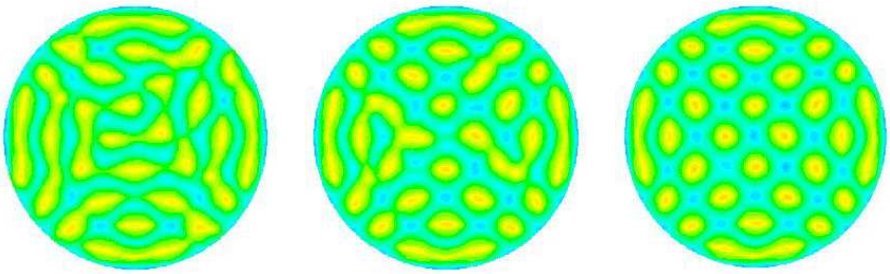

Figure 5.10: Time evolution of a spiral pattern in Rayleigh convection of magnetic fluid after magnetic field of $H = 48$ kA/m was turned on. $\Delta T = 5$ K. The time interval between the snapshots is 1 min.

explained the contradictions of the theory and experimental results by the influence of concentration gradients caused by gravity sedimentation of magnetic particles and their capability to exert a material stabilizing effect on convection instability in suitable conditions. (Bozhko et al., 2004). Besides, as experiments shown, the sedimentation of magnetic particle aggregates increases in the presence of magnetic field (Peterson and Kruger, 1997).

When $M_s = 48$ kA/m, the magnetic Rayleigh number is about 3×10^3 already at modest magnetic field strengths due to large values of M and ΔT, i.e. it is comparable and even exceeds the gravitational one, which for layer with rigid thermal-conductive boundaries is $Ra_{g,cr} = 1708$. In these conditions the destabilizing influence of magnetic field, is observed.

The typical flow patterns in the presence of transversal magnetic field are "zipper states" consisted of the convection rolls of any orientation, which randomly break up and then are again restored. Under fixed value of ΔT the wavenumber depends on the relative contribution of magnetic mechanism and increases with magnetic field. At small magnetic fields, the spontaneous formation of spiral rolls as in the case of zero fields may be observed. In Figure 5.11 (a) the spiral is observed in the left quadrant. Then it extends to separate convective cells (Figure 5.11 (b)) and new spiral curl appears again in the right quadrant in Figure 5.11 (c).

The white ring in peripheral regions of photographs is connected with the disturbing motion due to magnetic field nonuniformity in magnetic fluid caused by the boundaries of volume. The sidewall magnetic field gradient creates radial pondermotive force, which disturbs the mechanical equilibrium of the liquid and generates perturbation flow. When $\Delta T < \Delta T_{cr}$, the disturbing flow has toroidal form. For $\Delta T > \Delta T_{cr}$, the convection rolls in the vicinity of edges are elongated in radial direction, which is clearly visible in the simulated pattern shown in Figure 5.12. The radial straightening of rolls is connected with the existence of horizontal component of magnetic field gradient that arises because of retraction of force lines of magnetic field at transition from the air to the ferrocolloid.

Complications caused by the large magnetic field gradient near the domain boundaries were even more pronounced in the numerical simulations, and made the solution to converge very slowly. Figure 5.13 (a) shows simulated magnetic field gradient inside the calculation domain, when external field $H = 10$ kA/m was applied. Simulated field near the boundaries is essentially smoother than the real one. In Figure 5.13 (b) temperature contours for subcritical case $\Delta T < \Delta T_{cr}$ are shown. $T_{cr} \approx 4.2$ K is the critical temperature difference for the onset of Rayleigh convection under applied magnetic field of 13 kA/m. In subcritical regime, the fluid motion is entirely due to horizontal field gradient and the spatial range of the boundary effects is

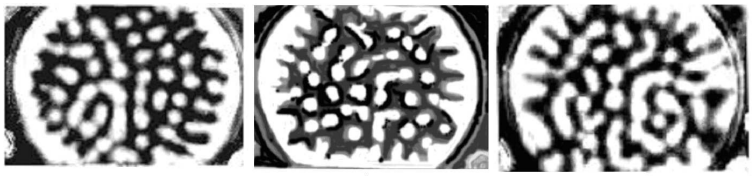

(a) (b) (c)

Figure 5.11: Convection patterns in horizontal ferrofluid layer heated from below and subjected to transversal magnetic field at $\Delta T/\Delta T_{\rm cr} = 1.5$ and $H = 10$ kA/m. The time interval between the snapshots is 5 min. Magnetic field is directed perpendicularly to the plane of photographs. Photos by Dr. A. Bozhko, PSU.

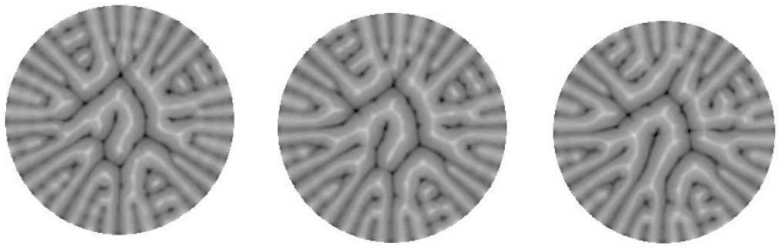

(a) (b) (c)

Figure 5.12: Simulated evolution of the spiral pattern. $H = 10$ kA/m and time interval between the snapshots is 2 min.

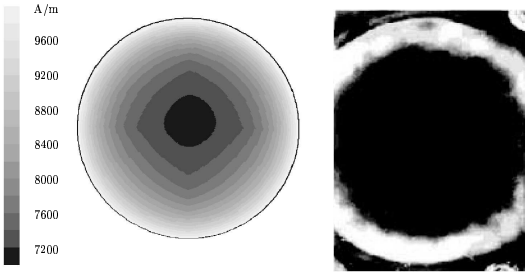

(a) (b)

Figure 5.13: (a) Magnitude of magnetic field inside the simulation domain for $H = 10$ kA/m. (b) Experimentally observed disturbing motion at subcritical regime for $H = 13$ kA/m and $\Delta T < \Delta T_{\rm cr}$. The temperature drop from cool (black) to warm (white) liquid is approximately 3 K. Photo by Dr. A. Bozhko, PSU.

approximately 10 % of the cell diameter, whereas in numerical simulations Figures 5.13 (a) and 5.12 the effect reaches almost to 30 % of the cell diameter. Steep gradients, would have required huge mesh densities near the domain boundaries, to correctly take into account the demagnetizing effects. Therefore in part of the simulations the sidewalls of the simulation domain were considered periodic and the magnetic field was allowed to change only in z-direction. Figure 5.10 presents simulated time evolution of the magnetic fluid convection after transversal magnetic field of $H = 48$ kA/m was turned on. The simulations have been conducted using previously mentioned magnetically periodic boundaries, which can be noticed from the absence of the radial disturbances next to boundaries. Although unrealistic close to domain boundaries, the method is computationally effective and in addition it captures the essential features and alignment of convection rolls with the applied field. For better results the experiments and numerical simulations should be conducted for disk with larger aspect ratio where the boundary effects are not so significant.

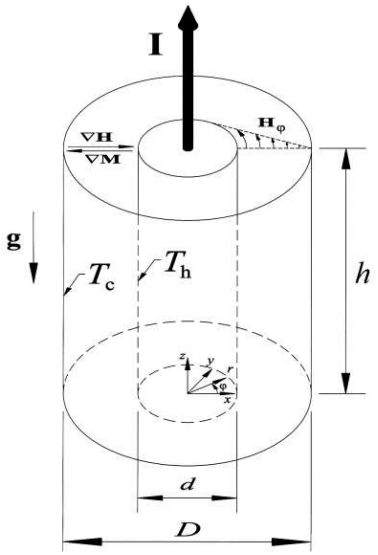

Figure 5.14: Problem geometry and the nomenclature used in the calculations.

5.2 Cylindrical annulus

Another studied geometry was an annular cavity between two concentric cylinders shown in Figure 5.14, Publication V, (Tynjälä and Ritvanen, 2004). Magnetic fluid is held in an annulus and the inner cylinder is kept at a higher temperature than the peripheral one. An electric current is led through the inner cylinder to produce an azimuthal magnetic field, decreasing in the radial direction. Because of the temperature dependence of the fluid magnetization a magnetization gradient opposite to the temperature gradient is generated.

When a fluid element with colder temperature and therefore higher magnetization is moved towards the inner cylinder it experiences a higher magnetic force than the warmer fluid surrounding it. This magnetic force is effecting in the direction of magnetic field gradient and tends to move the fluid element further towards the center of the cylinder leading to instability. The system is similar with the Rayleigh-Bernard convection of an ordinary fluid under a radial gravitational field.

In the absence of magnetic field gradient and in the presence of gravity, the buoyancy driven convection will take place, leading to purely meridional convection. Buoyancy driven convection in a cylindrical annulus has been studied e.g. by Lee et al. (1982). In the absence of gravity, the azimuthal convection with counter rotating cells takes place in an annulus, because of

the radial temperature and magnetic field gradients, and the temperature dependence of the fluid magnetization. This phenomenon has been studied earlier both by computational methods (Zebib, 1996) and by experiments under microgravity conditions (Odenbach, 1995).

Most of the classical studies, both in buoyancy driven convection (Gebhart et al., 1988), and thermomagnetic convection (Finlayson, 1970) are related to the two-dimensional plane and axisymmetric flows. However, the combination of magnetic convection caused by radial magnetic field gradient and natural convection caused by gravity vector parallel to the cylinder axis leads to complicated three-dimensional flow. Recently, it was shown that the onset of convection may be three-dimensional also in the absence of gravity (Zebib, 1996). In addition to two-dimensional approximation, two simplifications have often been made in the studies of thermomagnetic convection, namely the superposition of parallel or antiparallel gravitational and magnetic body forces, or the assumption of a strong magnetic field gradient and negligible gravitational convection. In this study the direction of the gravity and the magnetic field gradient are perpendicular to each other so that these two phenomena cannot be presented with a single effective body force term. Also the focus is mainly at the cases, where the contributions of magnetic and buoyant forces are of the same order of magnitude, and neither one is clearly dominant.

5.2.1 Problem setup

Magnetic field is produced by letting a constant current I through the inner cylinder. The magnitude of magnetic field and magnetic field gradient may then be written

$$H_0 = \frac{I}{2\pi r} \qquad \nabla H = -\frac{I}{2\pi r^2}\mathbf{e}_r. \tag{5.17}$$

The simulations were carried out for the 0.1 m high cylinder with the diameters of the inner and the outer cylinder equal to 0.010 and 0.022 m, respectively. Finite element method with single phase approximation presented in Chapter 4 was used in the simulations.

Prandtl number is a dimensionless number, which may be used to estimate the ratio of thermal and hydrodynamic boundary layer thicknesses. The free convection hydrodynamic boundary layer is made up of two parts. One in which the velocity rises and a region where the velocity decays to zero. In the case of magnetic fluids, when the Prandtl number is much more than unity, the thermal boundary layer is thinner than the hydrodynamic one. Still it is important to construct the mesh in a way that both parts of hy-

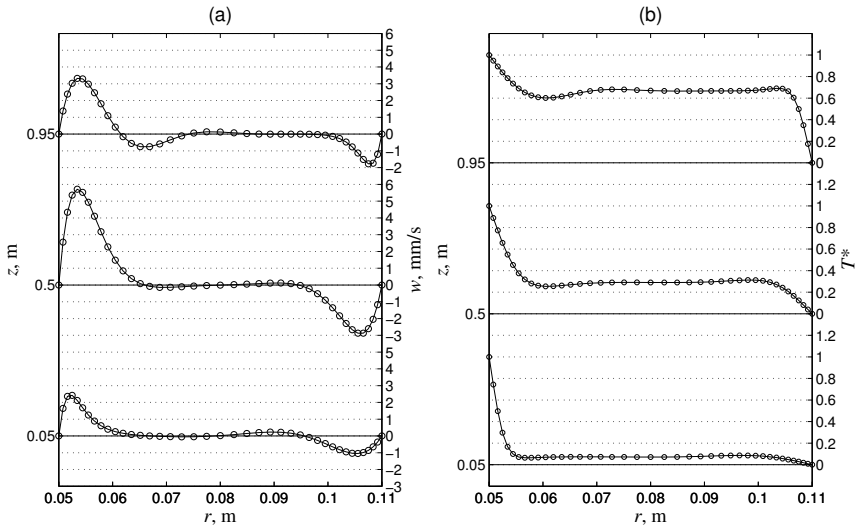

Figure 5.15: Distribution of (a) velocity in z-direction w and (b) dimensionless temperature T^* as a function of radius r taken from three different heights, namely $z = 0.05, 0.50, 0.95$ m, for gravitational and magnetic Rayleigh numbers equal to 7×10^5 and 3000, respectively.

drodynamic boundary layer as well as thermal boundary layer are captured. In Figure 5.15 the z-velocity distribution and the temperature distribution with gravitational and magnetic Rayleigh numbers equal to 7×10^5 and 3000, respectively, are shown.

In the simulations 40 grid points were used in radial direction. In the light of velocity and temperature boundary layers shown in 5.15, the amount of grid points in radial direction seems to be sufficient for the Rayleigh numbers under consideration. The number of grid points was 200 in the azimuthal and 150 in the vertical direction, leading to hexahedral mesh with 1 200 000 cells.

The physical properties of the studied ferrofluid were as follows: density $\rho = 1400$ kg/m^3, thermal expansion coefficient $\beta = 0.0002$ 1/K, kinematic viscosity $\nu = 1.3 \times 10^{-6}$ m^2/s, thermal diffusivity $\kappa = 1.3 \times 10^{-7}$ m^2/s, pyromagnetic coefficient $\beta_\mathrm{m} = 0.0002$ 1/K and the Prandtl number $Pr = 10$. All physical properties were considered constant and determined at average temperature and magnetic field.

Constant temperature boundary conditions were used for cylindrical surfaces. Top and bottom of the cylinder were insulated and no-slip boundary conditions were applied on all of the walls. Current I led through the in-

ner cylinder and temperature difference between the cylinders were varied in order to achieve the desired gravitational and magnetic Rayleigh numbers.

As an initial conditions for the time dependent calculations the base state in the absence of fluid motion $\mathbf{u} = 0$ was used. In the considered cylindrical geometry the solving of conduction equation leads to the radial temperature distribution of the form:

$$T(r) = T_{\mathrm{h}} - \frac{T_{\mathrm{h}} - T_{\mathrm{c}}}{\ln\left(\frac{D}{d}\right)} \ln\left(\frac{2r}{d}\right) \tag{5.18}$$

Characteristic time for reaching the quasi-steady state may be approximated (Odenbach, 1995) as $\tau = L^2/\nu$. In the analysis, the gravitational Rayleigh number Ra and the magnetic Rayleigh number Ra_m were defined as follows:

$$Ra = \frac{g\beta\Delta T L^3}{\nu\kappa} \qquad\qquad Ra_m = \frac{\mu_0\beta_{\mathrm{m}} M_0 \Delta T L^2 \Delta H}{\rho\nu\kappa} \tag{5.19}$$

where g is the acceleration of gravity, μ_0 is the vacuum permeability, L is a characteristic length equal to the gap width and ΔT and ΔH are the temperature and magnetic field differences over the gap. In the simulations both gravitational and magnetic Rayleigh numbers were varied between 0 and 10^6.

5.2.2 Simulations in the absence of gravity

At first, two-dimensional simulations were carried out for pure magnetic convection. Temperature and velocity contours of two-dimensional simulations are presented in Figures 5.18 and 5.19. In the absence of gravity two-dimensional simulations could reproduce the expected phenomena with counter rotating convection cells with diameter equal to the thickness of fluid layer. However, the onset of convection was found already with magnetic Rayleigh numbers about one thousand, which is much less than the theoretical (Zebib, 1996; Polevikov and Fertman, 1977) or experimental (Odenbach, 1995) predictions $Ra_{m,cr} \approx 1800$. Three-dimensional simulations were carried out in order to increase the accuracy of the two-dimensional simulations. In Figure 5.16, the average Nusselt number for the cylinder as a function of magnetic Rayleigh number has been presented. Dashed line in Figure 5.16 represents the experimental correlation (Berkovsky et al., 1980) for average Nusselt number $Nu_{\mathrm{av}} = 0.25 Ra_{\mathrm{m}}^{0.24}$.

It may be said that the results of three-dimensional steady-state simulations are in better agreement with the theoretical (Zebib, 1996) and experimental (Odenbach, 1995) predictions than two-dimensional, but the simula-

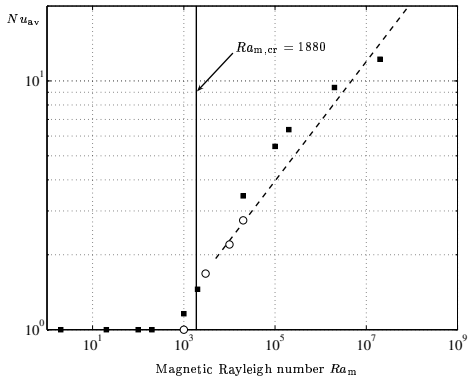

Figure 5.16: Average Nusselt number as a function of magnetic Rayleigh number. Squares and circles are the results of two and three-dimensional simulations in the absence of gravity, respectively, and the dashed line is drawn based on the correlation presented in (Berkovsky et al., 1980). Solid line shows the value for the critical magnetic Rayleigh number ($Ra_{m,cr} = 1880$) for the pure magnetic convection (Polevikov and Fertman, 1977).

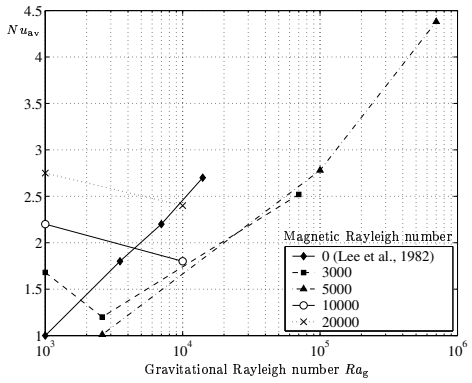

Figure 5.17: Average Nusselt numbers as a function of gravitational and magnetic Rayleigh numbers. The reference values for buoyancy driven convection (Lee et al., 1982), are also shown. Symbols at $Ra_g = 10^3$ refer to the case $Ra_g = 0$.

tions are very time consuming near the onset of instability, which makes the accurate prediction of critical Rayleigh number difficult.

5.2.3 Simulations in the presence of gravity

When the gravity perpendicular to the magnetic field gradient is introduced, the case becomes more complicated. The flow will be three-dimensional and in addition the flow may become unsteady consisting of upward drifting cells. Similar phenomena can be found when the buoyancy driven convection of ordinary fluids is studied in a vertical annulus. The cellular structure, which is stationary in a Cartesian geometry, drifts upward when the curvature is introduced (Lee et al., 1982). In natural convection the speed of rising cells has found to depend on the radius and aspect ratios of the cylinders as well as on the fluid properties, namely Prandtl number (Lee et al., 1982). In this study only the effect of the magnetic and gravitational Rayleigh numbers and their ratio, $N_\mathrm{m} = Ra_\mathrm{m}/Ra_\mathrm{g}$, on the convection was studied and other parameters, such as Prandtl number, radius ratio and aspect ratio, were kept constant.

The limiting values for the onset of pure buoyancy driven convection in a vertical annulus are (Schwab and DeWitt, 1970) $Ra_\mathrm{g} > 5 \times 10^3$ and $Ra_\mathrm{m} = 0$, and for pure thermomagnetic convection in the absence of gravity (Polevikov and Fertman, 1977), $Ra_\mathrm{m} > 1880$ and $Ra_\mathrm{g} = 0$. Based on the simulations, these values may be considered also as critical values for combined convection. There was no clear evidence that any combination of gravitational and magnetic Rayleigh numbers, both being smaller than these critical values, would give a significant increase to the heat transfer rate of the pure conduction. More like it looked that for small gravitational Rayleigh numbers the introduction of magnetic field gradient may stabilize the flow. Though, once again it must be said that the simulations near the onset of instability are very time consuming, and the number of trial cases was too small to accurately determinate the critical values for the onset of combined convection.

Unsteady simulations revealed that the speed of rising cells decreases when the ratio of magnetic and gravitational Rayleigh numbers is increased and for the ratio $N_\mathrm{m} > 100$ the steady azimuthal convection, similar to that of pure thermomagnetic convection, takes place. In the other end, when $N_\mathrm{m} < 0.05$, the convection may be considered to be buoyancy dominated and the effect of magnetic field may be neglected. Temporal evolution of the flow in a vertical plane of the annulus for the Rayleigh numbers $Ra_\mathrm{g} = 10^4$ and $Ra_\mathrm{m} = 10^4$ is shown in Figure 5.20.

However, the unsteadiness of the flow doesn't have much of an influence, when the average Nusselt numbers are calculated. In Figure 5.17 the average

Nusselt numbers as a function of gravitational and magnetic Rayleigh numbers have been plotted for selected cases. The values have been calculated based on a single time step after a quasi-steady state has been reached. Also some reference values for buoyancy driven convection (Lee et al., 1982), are shown.

5.2.4 Results and discussion

Computer simulations of the three-dimensional thermomagnetic convection have been performed in order to have a better understanding from the onset of magnetic convection and the relationship between the gravitational and magnetic convection. Necessary terms to describe the magnetic body force have been applied to the equation of momentum.

In the absence of gravity the flow consists of counter rotating convection cells in a horizontal plane. Two-dimensional computer simulations revealed the expected flow pattern and the magnitude of average heat transfer rate was close to the expected values. However, the two-dimensional simulations couldn't predict the correct value for the critical Rayleigh number with which the onset of convection occurs. Conducting the three-dimensional simulations improved the results somewhat, although the accurate simulation of the exact moment of the onset of instability is very time consuming. Recently Zebib (1996) studied the critical stages and stability of the thermal convection of magnetic fluid in a three dimensional cylindrical annulus. His analysis agreed well with the microgravity experiments of Odenbach (1995). In the analysis it was shown that there are competing states for the onset of instability. The linear theory predicts the onset of convection to be three-dimensional, with $Ra_{\mathrm{m}} = 1802.36$ and the two-dimensional azimuthal convection takes place when the magnetic Rayleigh number is further increased beyond $Ra_{\mathrm{m}} > 1900$.

In the presence of gravity, the convective motion will be three-dimensional and in addition it may be time dependent with cellular patterns drifting upwards. Reason for this phenomenon is thought to be the curvature of the cylindrical surface, which destroys the symmetry of the velocity profile (Lee et al., 1982). The simulations showed that the introduction of magnetic field gradient may stabilize the flow with small gravitational Rayleigh numbers and that convection may occur only, if either the critical magnetic Rayleigh number of pure thermomagnetic convection or the critical Rayleigh number of pure buoyancy driven convection is exceeded. The speed of rising cells decreases when the ratio of magnetic and gravitational Rayleigh numbers increases, leading to the steady azimuthal convection, when $N_{\mathrm{m}} > 100$.

Linear stability analysis of the buoyancy driven convection in a cylindrical annulus has revealed that the magnitude of Prandtl number has a major

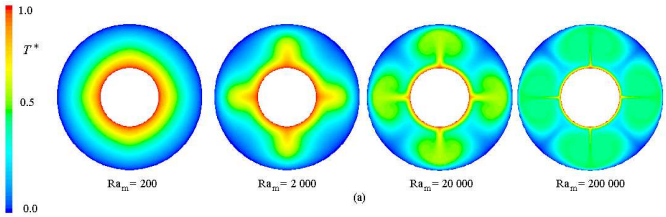

Figure 5.18: Temperature contours of thermomagnetic convection in the absence of gravity

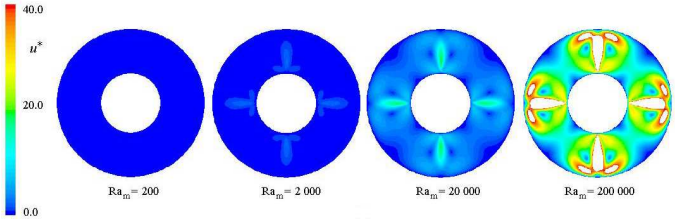

Figure 5.19: Velocity contours of thermomagnetic convection in the absence of gravity

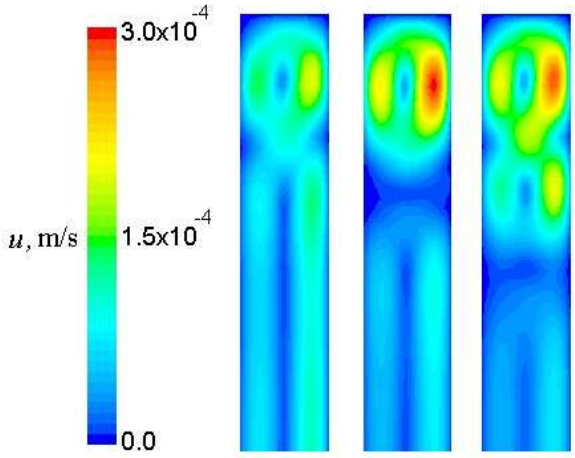

Figure 5.20: Temporal evolution of the flow in vertical plane of the annulus for the Rayleigh numbers $\mathrm{Ra} = \mathrm{Ra_m} = 10^4$.The time increment between successive plots $\Delta t = 5.0$s.

effect on the stability of the flow. As for low Prandtl numbers increasing the curvature of the annulus stabilizes the flow whereas the opposite is true for high Prandtl numbers (Lee et al., 1982). Prandtl numbers of a magnetic fluid vary greatly and magnetic fluids with very high Prandtl numbers are often considered. Therefore it is important to extend the future studies to include the effect of Prandtl number and radius ratio of the cylinders.

5.3 Triangular enclosure

An isosceles triangular enclosure was third studied geometry, Publication VI, (Tynjälä et al., 2002). Geometry of the studied case with nomenclature used and contours of constant induction field calculated from magnetostatic approximation, are presented in Figure 5.21. The case was selected to study the differences between the classical theoretical description due to Shliomis (1972) and the hydrodynamic approach of Liu (1993). Different treatment of magnetodissipation in above mentioned theories was discussed in detail by Müller and Engel (1999). The description by Shliomis (1972) uses a mesoscopic treatment of the particle motion to derive a relaxation equation for the nonequilibrium part of the magnetization. Complementary, the hydrodynamic approach of Liu (1993) involves only macroscopic quantities and results in dissipative Maxwell equations for the magnetic fields in the magnetic fluid.

The isosceles triangle geometry was selected since the ratio of the field intensity in the x- and z-directions may be controlled by changing the aspect ratio of the triangle and this way the differences between the two theories could be promoted. This technique was used to investigate differences in the results for the two theories, since the magnetic dissipation is isotropic for the mesoscopic theory and anisotropic for the hydrodynamic theory.

Recently, the free convection of ordinary gases and liquids in the same geometry has been studied experimentally (Holtzman et al., 2000). An excellent agreement was found, when the measured stream functions were compared with those obtained by simulations, in the absence of magnetic field.

5.3.1 Theoretical considerations and governing equations

Two different theories, namely mesoscopic and hydrodynamic, are used to express the fluid stress tensors. If the magnetic relaxation processes on the hydrodynamic time scales are not instantaneous, the treatment of the magnetodissipation using the aforementioned expressions leads to different governing equation of motion. If the magnetic fluid is treated as homogeneous

single fluid, and when all heat sources and magnetostriction of the particles are neglected (Bashtovoy et al., 1988), the continuity and energy equations are common for both theories and may be reduced to

$$\nabla \cdot \mathbf{u} = 0, \tag{5.20}$$

$$\rho c_{V,H}(\mathbf{u} \cdot \nabla T) = \lambda \nabla^2 T. \tag{5.21}$$

Different treatment of magnetodissipation leads to different momentum equations. Momentum equation for the mesoscopic theory is given by

$$\rho\,(\mathbf{u} \cdot \nabla \mathbf{u}) = -\nabla p - \rho\beta\nabla T g\mathbf{k} + \eta\nabla^2\mathbf{u} + \mu_0(\mathbf{M}\cdot\nabla)\mathbf{H} + \frac{\mu_0}{2}\nabla\times(\mathbf{M}\times\mathbf{H}), \tag{5.22}$$

and momentum equation for hydrodynamic theory by

$$\rho\,(\mathbf{u} \cdot \nabla \mathbf{u}) = -\nabla p - \rho\beta\nabla T g\mathbf{k} + \eta\nabla^2\mathbf{u} + \mu_0 M^R \nabla H^R + \mathbf{B}\times(\nabla\times\mathbf{H}^D), \tag{5.23}$$

where $\mathbf{H}^R$ and $\mathbf{H}^D$ refer to equilibrium and dissipative off-equilibrium part of field used in hydrodynamic theory and defined as

$$\mathbf{H} = \mathbf{H}^R + \mathbf{H}^D = \mathbf{H}^R + \tau_{\text{hydro}}(1+\chi)\left[(v\cdot\nabla)\mathbf{H}^R - (\mathbf{H}^R\cdot\nabla)v\right]. \tag{5.24}$$

For mesoscopic theory the magnetization relaxation can be written as a sum of equilibrium and off-equilibrium term as

$$\mathbf{M} = \chi\mathbf{H} + \delta\mathbf{M} = \chi\mathbf{H} - \tau_{\text{meso}}\chi\left[(u\cdot\nabla)\mathbf{H} - \frac{\nabla\times u}{2}\times\mathbf{H}\right]. \tag{5.25}$$

In Equations (5.25) and (5.24) τ_{meso} and τ_{hydro} represent characteristic relaxation times used in the mesoscopic and hydrodynamic theories defined in (Müller and Engel, 1999).

For the current case the terms accounting for the magnetodissipation in momentum equations may be simplified, expanding the last terms in Equations (5.22) and (5.23), with help of Equations (5.25) and (5.24). In addition, continuity condition $\partial u/\partial x = -\partial w/\partial z$ have been applied. Furthermore second derivatives of field, terms of order δ^2 and field magnitude in x-direction ($H_x \ll H_z$) have been neglected. These assumptions lead to following equations for magnetodissipative terms in momentum equations of two theories under consideration.

For the mesoscopic theory

$$\frac{\mu_0}{2}\nabla \times (\mathbf{M} \times \mathbf{H}) = \frac{\chi \mu_0 \tau_{\text{meso}}}{4} H_z^2 \nabla^2 \mathbf{u}, \tag{5.26}$$

and magnetodissipation in momentum equation may be combined with viscous term, replacing ordinary fluid viscosity η with the magnetic viscosity η_{m} defined as

$$\eta_{\text{m}} = 1 + \frac{\chi \mu_0 \tau_{\text{meso}}}{4} H_z^2. \tag{5.27}$$

For the hydrodynamic theory the equation for the magnetodissipation is not symmetric and similar viscosity term accounting for the magnetic contribution, as for the mesoscopic theory can't be written. Instead following term will appear in x-momentum equation

$$\mathbf{B} \times (\nabla \times \mathbf{H}^D) = \tau_{\text{hydro}} (1 + \chi)^2 \mu_0 H_z^2 \left(\frac{\partial^2 u}{\partial z^2} + \frac{\partial^2 u}{\partial x^2} \right). \tag{5.28}$$

5.3.2 Numerical model

Electrical conductivity of magnetic fluids is usually very small and often the fluids can be considered nonconductive. Magnetic field was calculated using magnetostatic solver and applying the simplified Maxwell equations for a non-conducting fluid (Rosensweig, 1997) given as follows

$$\nabla \cdot \mathbf{B} = 0 \tag{5.29}$$

$$\nabla \times \mathbf{H} = 0. \tag{5.30}$$

In order to avoid complications caused by considering the conditions on $\mathbf{B}$ and $\mathbf{H}$ at the boundaries of enclosure, the magnetic field within the ferrofluid is obtained by solving Equations 5.29 and 5.30 numerically over a rectangular domain where a uniform external field of $\mathbf{H}_0 = H_0 \mathbf{k}$, is applied at its boundaries. Here l represents the height of the triangular enclosure, H_0 is the magnetic field strength, and $\mathbf{i}$ and $\mathbf{k}$ represent the unit vectors in the x- and z-directions, respectively. Moreover, both the normal component of $\mathbf{B}$ and the tangential component of $\mathbf{H}$ are continuous passing through the walls of the enclosure that separates the ferrofluid from the air.

By using constant temperature boundary conditions, with $T = T_{\text{C}}$ at the sides and $T = T_{\text{H}}$ at the bottom of the enclosure, numerical solutions are obtained using the commercial code finite element solver Fidap.

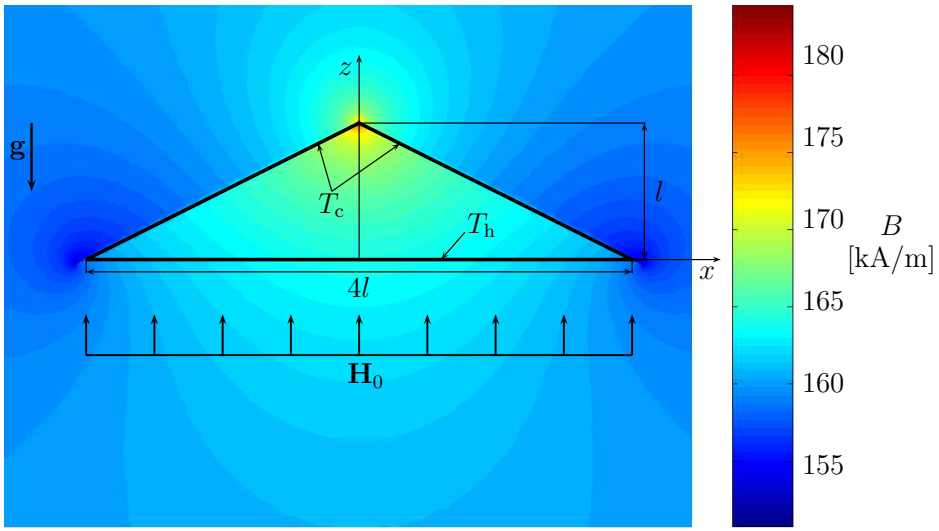

Figure 5.21: Geometry of the studied triangular isosceles enclosure. Contours represent magnitude of the induction field B calculated from magnetostatic approximation for isothermal case.

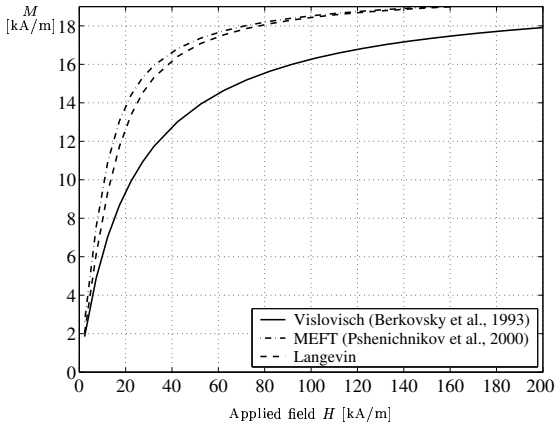

Figure 5.22: Magnetization curve of the studied ferrofluid calculated from Langevin theory (dashed), modified effective field theory (solid) and method suggested by Vislovich in (Berkovsky et al., 1993)

The magnetization of the ferrofluid is a function of temperature and the magnetic field. The magnetic equation of state is linearized about the applied magnetic field H_0 and the average temperature of the fluid T_0, to obtain $M = M_0 + \chi(H - H_0) - \beta_\mathrm{m} M_0(T - T_0)$, where χ is the differential susceptibility of ferrofluid and β_m is the pyromagnetic coefficient (Finlayson, 1970). The susceptibility χ, which is defined as M/H, may be estimated using the approximate method suggested by Vislovich in (Berkovsky et al., 1993). The magnetization curve of the ferrofluid under isothermal conditions is shown in Figure 5.23. For the conditions in which $\mu_0 mH/k_\mathrm{B}T \gg 1$ and at temperatures far from the Curie temperature, it may be approximated that $\beta_\mathrm{m} \approx \beta$ (Berkovsky et al., 1993), where β is the coefficient of thermal expansion of the carrier fluid.

The physical properties of the studied hydrocarbon based ferrofluid were as follows: density $\rho = 1110$ kg/m^3, heat conductivity $k = 0.154$ W/mK, thermal expansion coefficient $\beta = 0.00068$ 1/K, viscosity $\eta = 0.30$ kg/ms and the specific heat capacity $c_p = 1909$ J/kgK. Here the susceptibility of ferrofluid was assumed constant $\chi = 0.1$ corresponding to the external field of $H_0 = 165$ kA/m. Volume fraction of solid magnetite was 4.2 % which leads to saturation magnetization of 19.9 kA/m.

Using the results of the magnetic induction field as shown in Figure 5.21, steady-state simulations are performed to obtain the velocity and temperature fields of the magnetic fluid.

5.3.3 Results and discussion

In the simulations, when the ratio of the magnetic and gravitational Rayleigh numbers was held constant ($N_\mathrm{m} = Ra_\mathrm{m}/Ra_\mathrm{g} = 5.3$), it was observed that up to the critical value of gravitational Rayleigh number the flow field appears to be symmetric about the center axis of the triangle. If the Rayleigh number is further increased the symmetry may be destroyed. As shown in Figure 5.23 (a) the hydrodynamic theory predicts that the symmetry of the flow may break down at $Ra_\mathrm{g} = 1000$. However at the same Rayleigh number the mesoscopic theory suggest the regular roll cells, as depicted in Figure 5.23 (b). This discrepancy may be explained by considering the fact that magnetodissipation is treated differently by the two theories. For larger Rayleigh numbers the differences in the convection patterns are more pronounced. Figure 5.24 shows streamline predictions for both theories for $Ra_\mathrm{g} = 2 \times 10^4$ and $N_\mathrm{m} = 1.7$. Differences of heat fluxes calculated from different theories are presented in Figure 5.25, where the Nusselt numbers for studied cases have been presented as a function of gravitational Rayleigh number and ratio of magnetic and gravitational Rayleigh numbers.

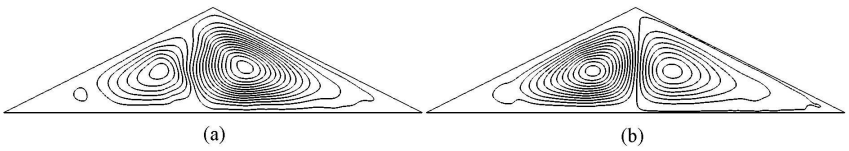

Figure 5.23: Streamlines for the magnetic convection predicted by (a) the hydrodynamic theory and (b) the mesoscopic theory, for $Ra_{\mathrm{g}} = 1000$ and $Ra_{\mathrm{m}} = 5300$.

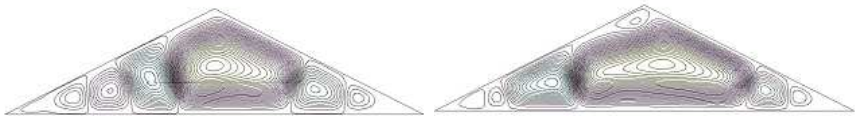

Figure 5.24: Streamlines for the magnetic convection predicted by (a) the hydrodynamic theory and (b) the mesoscopic theory for $Ra_{\mathrm{g}} = 2 \times 10^4$ and $N_{\mathrm{m}} = 1.7$.

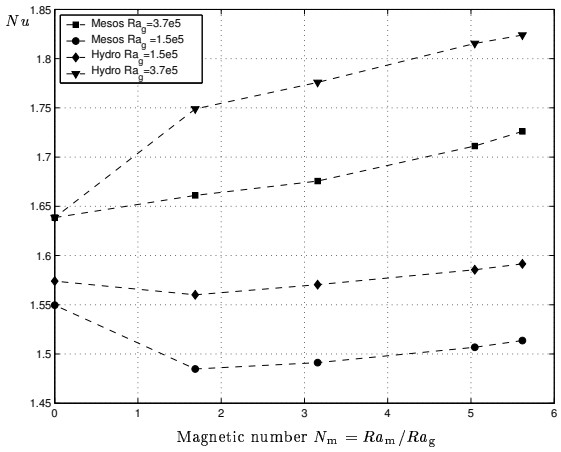

Figure 5.25: Nusselt number as a function of ratio of magnetic and gravitational Rayleigh numbers, for simulated cases with hydrodynamic theory and mesoscopic theory for gravitational Rayleigh numbers 1.5×10^5 and 3.7×10^5.

Clearly, experimental observations are required in order to assess the validity of the numerical results obtained using the hydrodynamic and mesoscopic theories. The isosceles triangle geometry is well suited for visual observations of the flow field since the deformation of the symmetric convection cells may be captured, although the evaluation of the field inside of the triangle may prove to be quite challenging.

In principle, both methods should give approximately same results and the effect of magnetodissipation in this case should be negligible. In the simulations, the relaxation time has perhaps little underestimated, which makes the effect of magnetodissipation more pronounced. However, the fundamental difference in governing equations and in the simulation results indicates that if the method suggested by Liu (1993) is used, the governing equations should be modified accordingly to take into account the antisymmetric stress tensor. In principle, this can be done by applying appropriate counter forces and coefficients determined by the Onsager reciprocal relations (Onsager, 1931a,b; de Groot, 1951) Equation (2.14). Applying this in practice may be challenging because of difficulties in the determination of correct phenomenological coefficients for various magnetic fluids.

6 Conclusions

In the previous chapters, the results and discussions sections have been provided for each studied case separately. This chapter concludes the work and presents some ideas about the future challenges.

In this study magnetic field control of convection instabilities and heat and mass transfer in magnetic fluids, composed of single domain particles of magnetic material suspended in a liquid carrier, have been investigated. The properties and behavior of complex multiphase systems have been considered theoretically and numerical studies of magnetic fluid convection in a triangular, cylindrical and shallow circular cavity, have been carried out for different magnetic field configurations.

Simulation methods based on finite element and finite volume methods have been developed. Simulation models have been built on top of commercial Fidap (Finite Element Method) and Fluent (Finite Volume Method) softwares. In addition to standard conservation equations, the magnetic field inside the simulation domain is calculated from the Maxwell equations and the necessary terms to take into account the magnetic body force and magnetic dissipation have been added to the governing equations. Simulations have been carried out by using both a single phase and a two-phase mixture model. In the mixture model simulations the conservation equations for mass, momentum and energy are solved for the mixture phase, and relative velocity between the fluid and the particles is calculated from an algebraic expression. Simulation models have been tested against available experimental results and qualitatively good results have been achieved.

For dense magnetic fluids near the onset of convection, the competitive action of thermal and concentration density gradients mostly leads to spatiotemporally chaotic convection, previously observed in binary mixtures and nematic liquid crystals. Oscillatory convection was observed in the entire investigated temperature region and different wave regimes, such as spirals, targets, rolls and cross-rolls, were discovered. For magnetic fluids with low particle concentration, or if the single phase approximation was used in the simulations, steady convection rolls were discovered.

In order to study the nature of spatiotemporal variations of temperature oscillations, wavelet analyses have been conducted for experimental temperature signals. The wavelet-analysis revealed that along with periods of 8 to 15 minutes there are longer periods from a few to several hours. The existence of long and short periods is typical for magnetic fluid convection. As to the time evolution of patterns, there is slow movement of the roll systems as a whole because of the mean flow, and "high-speed" reconstruction of the convection rolls due to the cross-roll instability.

Experimentally observed hysteresis and strong dependence of the measured heat flux on the prehistory of the experiments alludes to a non-newtonian nature of magnetic fluids. The depth of the hysteresis loop depends on the prehistory of the experiment and is wider for initially non-mixed fluid than for convection mixed fluid, which testifies the presence and breaking of the aggregates in the fluid.

Based on numerical simulations, the size of the drop aggregates, which could lead to experimentally observed sedimentation, was found to be the order of 100 nm or larger, which is clearly more than the commonly accepted value for magnetic fluids of good quality. Numerical simulations of magnetic fluid convection near the threshold supported experimental observations qualitatively. For single phase cases, conducted in cylindrical annulus, the predictions for the onset of convection were also quantitatively in good agreement with the theoretical predictions. Simulations near the threshold are time consuming and slow motions of unsteady behavior are difficult to observe. In addition to the long computing time needed for the simulations near the threshold, problems arise also because of the limited memory capacity to store unsteady simulation data.

Despite years of theoretical studies, the experiments in this region are not numerous. Detailed comparison of simulation results with the experiments is often problematic because of the lack of information about the fluid properties. If commercial magnetic fluids are used in the experiments, detailed information about the fluid properties is rarely available. Even if the fluids are synthesized and analyzed by the laboratory where the experiments are performed, the magnetic fluid particles are not monodisperse and the fluid properties are averaged mean values. However, the experiments with commercial magnetic fluids have shown that the increase in field-dependent viscosity is higher that one would theoretically expect based on the size distribution of particles in the fluid. The explanation for this phenomenon has been thought to be related to the pronounced effect of magnetically hard large particles and their aggregates, which may contain thousands of particles.

Another fact which makes the comparison of the results difficult is the number of various mechanisms, such as thermomagnetic and buoyancy driven convection and ordinary, thermal and magnetic diffusions, present in the system. To avoid complications caused by the uncontrollable gravitational sedimentation of magnetic particles present in terrestrial conditions, the experiments should be carried out in the absence of gravity. There exists some experimental studies conducted in a low-g environment, but the duration in most experiments is not long enough to show the slow movement of convection rolls observed in the experiments in terrestrial conditions and in the numerical simulations. For more detailed analysis of heat and mass transfer

phenomena in magnetic fluids as well as in other binary mixtures, long term experiments in a microgravity environment would be crucial. For example the following low-g investigations would shed light on heat and mass transfer mechanisms in magnetic fluids:

- Thermal and concentration magneto-convection without gravitational sedimentation, which strongly influences convection in terrestrial conditions.
- Measurement of Soret coefficients under microgravity conditions.
- Measurement of "pure" heat and mass diffusion coefficients under weightless conditions.

There is also still not clear understanding about the complex theory behind the heat and mass transfer in magnetic fluids. For example the values of the Soret and magnetic Soret coefficient, responsible for the thermal and magnetic diffusion in magnetic fluids, have been the subject of controversy. There is no full agreement even about the signs of these coefficients and order of magnitude estimate evaluations presented by different scientist may vary by a couple of orders.

Since its inception in the 1960's, huge development has taken place in magnetic fluids research, but the theories are still far from being complete. New applications for these fascinating fluids are still being introduced. Trends in the recent development of science have been directing the studies towards smaller and smaller systems, and fields such as nanotechnology and biotechnology offer interesting possibilities for the use of these controllable fluids. Numerical simulations are one tool in developing and testing the theories on magnetic fluids. Good experimental results are always needed and the experiments are becoming more complicated as the size of the studied systems is decreasing. Numerical simulations also offer a feasible tool for the product development, with which part of the expensive experiments may be replaced.

There exist a number of possible applications for the thermomagnetic convection of magnetic fluids. One application is heat transfer enhancement in microgravity applications, where the buoyancy driven convection is absent. Other one is cooling of power electronic components, where the temperature and magnetic field gradients, such as those presented in this study, are often inherent. In addition to magnetic fluids, the results and the simulation models developed in this study may be applied also to other binary mixtures, or numerical studies of free convection instabilities in any ordinary fluid.

7 Epilogue

In order to deal with the complex world around us, we need to have some ways to categorize it and explain the mysteries to ourselves. Physics is one way to do this and throughout the history, the scientists have tried to model the behavior of nature by a set of simple rules. Things that cannot be explained by the means of science have been left to God or ignored. It is good to remember that the nature does not need any laws to function. If the physical description of some phenomenon is more complex than the phenomenon itself, it can be said that the physicists have failed in their efforts to explain the world to us.

During the past decades, the term complexity has become popular in many areas of science. Besides physics, complexity can be found in economics, logistics as well as in evolutionary and biological systems. Often complex systems in totally different fields may have surprisingly similar features. Stock markets may show same trends, such as the population dynamics of some bacteria. The research of complexity is therefore an interesting and interdisciplinary topic, where an open-minded economist may have a lot to learn from the results of biochemistry and vice versa.

According to one definition, complexity means that we have a structure with variations. If we look at the world around us, we may say that the nature has a tendency toward the formation of structures. Partly, the beauty can be in the eye of the beholder, and the human mind is just willing to see ordered structures, as it is looking for the laws of nature. Nature can produce complex structures and obey simple laws even in simple situations (Goldenfeld and Kadanoff, 1999).

Fractals are examples of systems, which are generated by a set of simple laws. Many natural phenomena where ordered structures are present, such as the formation of a snowflake, diffusion limited growth (Witten and Sander, 1981) or growth of a plant, have been modeled using fractals. Figure 7.1 (a) shows an example of a fractal called "Barnsley's fern" (Barnsley, 1988) created using a simple algorithm. Looking at this fractal fern alone, we may say that it looks exactly like a real one. Going out and looking at a real fern, shown in Figure 7.1 (b), the diversity of the real world can be easily seen. Differences between the reality and imitating fractals can be taught more generally when mathematical modeling of physical systems is considered. Nature just exists, it does not obey the rules of nature. It depends on the application and the precision required whether we are happy with the result produced by the fractal or any other numerical model used to describe the system under consideration.

The term chaos is also mentioned often when complex systems are considered. According to one definition, chaos is the sensitive dependence of a final result upon the initial conditions that bring it about (Goldenfeld and Kadanoff, 1999). In a way, this brings us back to Heisenberg's principle (Heisenberg, 1927). In a chaotic world, it is impossible to know the initial conditions accurately enough to predict which variation will arise in a given place and time. The butterfly effect (Lorenz, 1963) is a common example of chaotic behavior. In the case of a fern, a more concrete example could be the "caterpillar effect": a butterfly larva may change the course of nature and destroy the fractal pattern by coming and having a bite ...

Figure 7.1: (a) Fractal *" Barnsley's fern"* created by a set of simple laws (Barnsley, 1988) and (b) a fern created by nature.

References

Ackerson, B. J. and Clark, N. A. (1981). Shear-induced melting. *Physical Review Letters*, 46:123–126.

Assenheimer, M. and Steinberg, M. (2000). Rayleigh-Bernard convection near the gas-liquid critical point. *Physical Review Letters*, 70:3888–3891.

Bacri., J. C., Perzynski, R., Shliomis, M. I., and Burde, G. I. (1995). "Negative-viscosity" effect in a magnetic fluid. *Physical Review Letters*, 75:2128–2131.

Barnsley, M. (1988). *Fractals everywhere*. Academic Press, Boston.

Bashtovoy, V. G., Berkovsky, B. M., and Vislovich, A. N. (1988). *Introduction to Thermomechanics of Magnetic Fluids*. Hemisphere Publishing Corporation, Washington.

Berkovsky, B. M., Fertman, V. E., Polevikov, V. K., and Isaev, S. V. (1980). Specific features of natural convection heat transfer in magnetic fluids. *IEEE Transactions on Magnetics*, 16:147–151.

Berkovsky, B. M., Medvedev, V. F., and Krakov, M. S. (1993). *Magnetic Fluids Engineering Applications*. Oxford Science Publication, Oxford.

Bestehorn, M., Friedrich, R., and Haken, H. (1980). Pattern formation in convective instabilities. *International Journal of Modern Physics B*, 4(3):345–400.

Bird, R. B., Stewart, W. E., and Lightfoot, E. N. (1960). *Transport phenomena*. John Wiley & Sons, New York.

Blums, E. (1995). Some new problems of complex thermomagnetic and diffusion-driven convection in magnetic colloids. *Journal of Magnetism and Magnetic Materials*, 149:111–115.

Blums, E. (2002). Heat and mass transfer phenomena. *Journal of Magnetism and Magnetic Materials*, 252:189–193.

Blums, E. (2005). New transport properties of ferrocolloids: magetic Soret effect and thermomagnetoosmosis. *Journal of Magnetism and Magnetic Materials*, 289:246–249.

Blums, E., Maiorov, M. M., and Tsebers, A. (1989). *Magnetic Fluids*. Zinatne, Riga.

Blums, E., Mezulis, A., Maiorov, M., and Kronkalns, G. (1997). Thermal diffusion of magnetic nanoparticles in ferrocolloids: Experiments on particle separation in vertical columns. *Journal of Magnetism and Magnetic Materials*, 169:220–228.

Blums, E. and Odenbach, S. (2000). Thermophoretic separation of ultrafine particles in ferrofluids in thermal diffusion column under the effect of an MHD convection. *International Journal of Heat and Mass Transfer*, 43:1637–1649.

Bogatyrev, G. P. and Shaidurov, G. F. (1976). Convection stability of a horizontal ferrofluid layer in the presence of homogeneous magnetic field. *Magnetohydrodynamics*, (3):137–146.

Bozhko, A. A. and Putin, G. F. (1991). Experimental investigation of thermomagnetic convection in an external uniform field. In *Proceedings of the Academy of Sciences. Physics*, volume 55, pages 1149–1155.

Bozhko, A. A. and Putin, G. F. (2003). Heat transfer and flow patterns in ferrofluid convection. *Magnetohydrodynamics*, 39:147–168.

Bozhko, A. A., Putin, G. F., Bulychev, P., Tynjälä, T., and Sarkomaa, P. (2005). Experimental and numerical study of oscillatory convection in ferrofluids. In *Joint 15th Riga and 6th PAMIR International Conference on Fundamental and Applied MHD, Vol. 1*, pages 337–340, Riga Jurmala, Latvia.

Bozhko, A. A., Putin, G. F., and Tynjälä, T. (2004). Oscillatory regimes of rayleigh convection in ferrofluid. In *Notices of Universities, South of Russia, Natural Sciences, Special Issue*, pages 68–73, Rostov-na-Donu. Rostov State University.

Bozhko, A. A. and Tynjälä, T. (2005). Influence of sedimentation of magnetic particles on ferrofluid convection in experiments and numerical simulations. *Journal of Magnetism and Magnetic Materials*, 289C:281–284.

Buzmakov, V. M. and Pshenichnikov, A. F. (1996). On the structure of microaggregates in magnetite colloids. *Colloid Interface Science*, 182:63–70.

Creus, G. J. (1986). *Viscoelasticity - Basic Theory and Applications to Concrete Structures*. Springer-Verlag, Berlin.

Daniels, K. E., Plapp, B. B., and Bodenschatz, E. (2000). Pattern formation in inclined layer convection. *Physical Review Letters*, 84:5320–5323.

Daubechies, I. (1990). The wavelet transform, time-frequency localization and signal analysis. *IEEE Transactions on Information Theory*, 36:961–1005.

de Groot, S. R. (1951). *Thermodynamics of irreversible processes*. North-Holland Publishing Company, Amsterdam.

Dennin, M., Ahlers, G., and Cannell, D. S. (1996). Chaotic localized states near the onset of electroconvection. *Physical Review Letters*, 77:2475–2478.

Einstein, A. (1906). On the movement of small particles suspended in a stationary liquid demanded by the molecular kinetic theory of heat. *Annalen der Physik*, 17:549.

Farge, M. (1992). Wavelet transforms and their applications to turbulence. *Annual Review of Fluid Mechanics*, 24:395–457.

Fauve, S. and Laroch, C. (1984). Spatial instabilities and temporal chaos. In Wesfreid, J. E. and Zaleski, S., editors, *Cellular structures in instabilities*, pages 278–284, Berlin. Springer.

Fertman, V. E. (1990). *Magnetic Fluids Guidebook: properties and applications*. Hemisphere Publishing Corporation, New York.

Fidap (1998). *Theory manual*. Fluent Inc., Lebanon.

Finlayson, B. A. (1970). Convective instability of ferromagnetic fluids. *Journal of Fluid Mechanics*, 40:753–767.

Fluent (2004). *Gambit 2.2 Users Guide*. Fluent Inc., Lebanon.

Fluent (2005). *Fluent 6.2 Users Guide*. Fluent Inc., Lebanon.

Gebhart, B., Jaluria, Y., Mahajan, R. L., and Sammakia, B. (1988). *Buoyancy-induced Flows and Transport*. Hemisphere Publishing Corporation, New York.

Getling, A. V. (1998). *Rayleigh-Bernard Convection: Structures and Dynamics*. World Scientific, Singapore.

Gluhov, A. and Putin, G. (1999). *Hydrodynamics*, volume 12. Perm State University, Perm.

Goldenfeld, N. and Kadanoff, L. P. (1999). Simple lessons from complexity. *Science*, 284:87–89.

Heisenberg, W. (1927). Über den anschaulichen Inhalt der quantentheoretische Kinematik und Mechanik. *Zeitschrift für Physik*, 43:172–198.

Holtzman, G. A., Hill, R. W., and Ball, K. S. (2000). Laminar natural convection in isosceles triangular enclosures heated from below and symmetrically cooled from above. *ASME Journal of Heat Transfer*, 122:485–491.

Huke, B. and Lücke, M. (2005). Roll, square, and cross-roll convection in ferrofluids. *Journal of Magnetism and Magnetic Materials*, 289:264–267.

Jaeger, H. M. and Nagel, S. R. (1992). Physics of the granular state. *Science*, 255:1523–1531.

Jalali, P. (2000). *Mass transfer and particle interactions in granular systems and suspension flows*. PhD thesis, Lappeenranta University of Technology, Espoo, Finland.

Jalali, P., jr. Polashenski, W., Tynjälä, T., and Zamankhan, P. (2002). Particle interactions in a dense monosized granular flow. *Physica D*, 162:188–207.

Jalali, P., Ritvanen, J., and Sarkomaa, P. (2005). Transient and steady state behaviors of rapid granular shear flows. *Experiments in Fluids*, 39:552–561.

Kubo, R. (1965). *Statistical Mechanics - An advanced Course with Problems and Solutions*. Elsevier Sciense Publishers, Amsterdam.

Lapple, C. E. (1961). Characteristics of particles and particle dipersoids. *Stanford Research Institute Journal*, 5:95.

Lederman, M., Schultz, S., and Ozaki, M. (1994). Measurement of the dynamics of the magnetization reversal in individual single-domain ferromagnetic particles. *Physical Review Letters*, 73:1986–1989.

Lee, J. F., Sears, F. W., and Turcotte, D. L. (1973). *Statistical Thermodynamics*. Addison-Wesley Publishing Company, Inc., Philippines.

Lee, Y., Korpela, S. A., and Horne, R. N. (1982). Structure of multicellular natural convection in a tall vertical annulus. In Grigul, U., Hahne, E., Stephan, K., and Straub, J., editors, *IHTC 7: Proceedings of the 7th International Heat Transfer Conference*, pages 221–226, Washington, DC. Hemisphere Publishing Corporation.

Lenglet, J., Bourdon, A., Bacri, J. C., and Demouchy, G. (2002). Thermodiffusion in magnetic colloids evidenced and studied by forced rayleigh scattering experiments. *Physical Review E*, 65:031408–1–14.

Liu, M. (1993). Hydrodynamic theory of electromagnetic fields in continuous media. *Physical Review Letters*, 70:3580–3583.

Lorenz, E. N. (1963). Deterministic nonperiodic flow. *Journal of the Atmospheric Sciences*, 20:130–141.

Manninen, M., Taivassalo, V., and Kallio, S. (1996). *On the mixture model for multiphase flow*. VTT Publications 288, Espoo, Technical Research Centre of Finland.

Maxwell, J. C. (1881). A treatise on electricity and magnetism. 1. §314.

McTague, J. P. (1969). Magnetoviscosity of magnetic colloids. *Journal of Chemical Physics*, 51:133–136.

Mekhonoshin, V. V. and Lange, A. (2004). Chain-induced effects in the faraday instability on ferrofluids in a horizontal magnetic field. *Physics of Fluids*, 16:925–935.

Müller, H. W. and Engel, A. (1999). Dissipation in ferrofluids: Mesoscopic versus hydrodynamic theory. *Physical Review E*, 60:7001–7009.

Müller, H. W. and Liu, M. (2001). Structure of ferrofluid dynamics. *Physical Review E*, 64:061405–1–061405–7.

Morris, S. W., Bodenschatz, E., Cannell, D. S., and Ahlers, G. (1996). The spatio-temporal structure of spiral-defect chaos. *Physica D*, 97:164–179.

Odenbach, S. (1995). Sounding rocket and drop tower experiments on thermomagmetic convection in magnetic fluids. *Advances in Space Research*, 16:(7)99–(7)104.

Onsager, L. (1931a). Reciprocal relations in irreversible processes. i. *Physical Review*, 37:405–426.

Onsager, L. (1931b). Reciprocal relations in irreversible processes. ii. *Physical Review*, 38:2256–2279.

Patankar, S. V. (1980). *Numerical heat transfer and fluid flow*. Hemisphere Publishing Corporation, Washington.

Patankar, S. V. and Spalding, D. B. (1972). A calculation procedure for heat, mass and momentum transfer in three-dimensional parabolic flows. *International Journal of Heat and Mass Transfer*, 15:1787–1806.

Peterson, E. and Kruger, D. A. (1997). Reversible, field induced agglomeration in magnetic colloids. *Journal of Colloids and Interface Science*, 62:24–33.

Pode, V. and Minea, R. (2000). Applications of magnetic fluids in heat transfer. In Maron, D. M., editor, *Book of Abstracts – Multiphase Flow and Transport Phenomena*, pages 58/1–5, Antalaya, Turkey.

Polevikov, V. K. and Fertman, V. E. (1977). Investigation of heat transfer through a horizontal annular layer of a magnetic liquid for the cooling of a cylindrical conductor with a current. *Magnetohydrodynamics*, 13:11–16.

Pshenichnikov, A. F. and Mekhonoshin, V. V. (2000). Equilibrium magnetization and microstructure of the system of superparamagnetic interacting particles: numerical simulation. *Journal of Magnetism and Magnetic Materials*, 213:357–369.

Raikher, Y. L. and Rusakov, V. V. (2003). Theoretical models for ac-field probing of complex magnetic fluids. *Journal of Magnetism and Magnetic Materials*, 258-259:459–463.

Raikher, Y. L., Stepanov, V. I., Bacri, J.-C., and Perzynski, R. (2005). Orientational dynamics in magnetic fluids under strong coupling of external and internal relaxations. *Journal of Magnetism and Magnetic Materials*, 289:222–225.

Rosensweig, R. E. (1997). *Ferrohydrodynamics. 2nd ed.* Dover Publications Inc., New York.

Rosensweig, R. E., Browaeys, J., Bacri, J.-C., Zebib, A., and Perzynski, R. (1999). Laboratory study of spherical convection in simulated central gravity. *Physical Review Letters*, 83:4904–4907.

Ryskin, A., Müller, H. W., and Pleiner, H. (2003). Thermal convection in binary fluid mixtures with a weak concentration diffusivity, but strong solutal buoyancy forces. *Physical Review E*, 67:046302–1–8.

Ryskin, A. and Pleiner, H. (2004). Influence of a magnetic field on the soret-effect-dominated thermal convection in ferrofluids. *Physical Review E*, 69:046301–1–10.

Schwab, T. H. and DeWitt, K. J. (1970). A numerical investigation of free convection between two vertical coaxial cylinders. *AIChE Journal*, 16:1005–1010.

Shliomis, M. I. (1972). Effective viscosity of magnetic suspensions. *Soviet Phys JETP*, 34:1291–1294.

Shliomis, M. I. and Morozov, K. I. (1994). Negative viscosity of ferrofluid under alternating magnetic field. *Physics of Fluids*, 6:2855–2861.

Shliomis, M. I. and Smorodin, B. L. (2002). Convective instability of magnetized ferrofluids. *Journal of Magnetism and Magnetic Materials*, 252:197–202.

Sikiö, P. (2004). Wavelet analysis in turbulence. Master's thesis, Lappeenranta University of Technology, Department of Energy and Environmental Technology.

Sykulski, J. K. and Stoll, R. L. (1995). A brief review of magnetic fields. In Sykulski, J. K., editor, *Computational Magnetics*, pages 1–34, London. Chapman & Hall.

Thurm, S. and Odenbach, S. (2002). Magnetic separation of ferrofluids. *Journal of Magnetism and Magnetic Materials*, 252:247–249.

Torquato, S. (2002). *Random heterogeneous materials: microstructure and macroscopic properties*. Springer-Verlag, New York.

Torquato, S., Truskett, T. M., and Debenedetti, P. G. (2000). Is random close packing of spheres well defined? *Physical Review Letters*, 84:2064–2067.

Tynjälä, T., Bozhko, A. A., Bulychev, P., Putin, G. F., and Sarkomaa, P. (2005). On features of ferrofluid convection caused by barometrical sedimentation. volume submitted.

Tynjälä, T., Hajiloo, A., Polashenski, W., and Zamankhan, P. (2002). Magnetodissipation in ferrofluids. *Journal of Magnetism and Magnetic Materials*, 252:123–125.

Tynjälä, T. and Ritvanen, J. (2004). Simulations of thermomagnetic convection in an annulus between two concentric cylinders. *Indian Journal of Engineering & Material Sciences*, 11:283–288.

Vecsey, L. (2002). *Chaos in thermal convection and the wavelet analysis of geophysical fields*. PhD thesis, Charles University, Prague, Czech Republic.

Völker, T. and Odenbach, S. (2005). Thermodiffusion in magnetic fluids. *Journal of Magnetism and Magnetic Materials*, 289:289–291.

Witten, T. A. J. and Sander, L. M. (1981). Diffusion-limited aggregation, a kinetic critical phenomenon. *Physical Review Letters*, 47:1400–1403.

Zahn, M. (2001). Magnetic fluid and nanoparticle applications to nanotechnology. *Journal of Nanoparticle Research*, 3:73–78.

Zamankhan, P. (2004). *Complex flow dynamics in dense granular flows*. PhD thesis, Lappeenranta University of Technology, Lappeenranta, Finland.

Zamankhan, P., Tynjälä, T., Polashenski, W., Zamankhan, P., and Sarkomaa, P. (1999). Stress fluctuations in continuously sheared dense granular materials. *Physical Review E*, 60:7149–7156.

Zebib, A. (1996). Thermal convection in a magnetic fluid. *Journal of Fluid Mechanics*, 321:121–136.

Zeuner, A., Richter, R., and Rehberg, I. (1998). Experiments on negative and positive magnetoviscosity in an alternating magnetic field. *Physical Review E*, 58:6287–6293.

Zuzovsky, M. and Brenner, H. (1977). Effective conductivities of composite materials composed of cubic arrangements of spherical particles embedded in an isotropic matrix. *Journal of Applied Mathemathics and Physics*, 28/6:979–992.